117 (2023) 205072

Contents lists available at ScienceDirect

Gas Science and Engineering

journal homepage: www.journals.elsevier.com/gas-science-and-engineering

# Conditions and thermophysical properties for transport of hydrocarbons and natural gas at high pressures: Dense phase and anomalous supercritical state

Laura M. Almara [a], Guo-Xiang Wang [b], Vish Prasad [a,*]

[a] University of North Texas, Department of Mechanical Engineering, UNT Discovery Park, Denton, TX, 76207-7102, USA
[b] The University of Akron, Department of Mechanical Engineering, Akron, OH, 44325, USA

ARTICLE INFO

*Keywords:*
Anomalous behavior
Gray zone for SC transport
Natural gas pipeline
Safe conditions
Supercritical hydrocarbons
Supercritical natural gas

ABSTRACT

Hydrocarbons and natural gas, like other fluids exhibit anomalous behavior in the vicinity of their critical points ($P_c$, $T_c$), where flow oscillations, thermal instabilities, and decreased heat transfer can occur. This work, based on Peng-Robinson equations of state, demonstrates that in the case of mixtures, the cricondenbar, cricondentherm, and a part of the dense phase belong to this anomalous region. Consequently, the most desirable conditions for the transport of supercritical natural gas (SNG) are: above the critical pressure and critical temperature, above the cricondenbar and cricondentherm, and beyond the anomalous state. For methane, such conditions exist at pressure, $P > 5$ MPa and temperature, $T >$ - 30 °C whereas for average composition of natural gases from US/Canada, West Asia, and North Sea, $P \geq 6$ MPa and $T > -30$ °C may be appropriate/safe for SNG transport. Corresponding gray zones which will require special design considerations are also identified. Reduced pressure, ($P/P_c$) of 1.15 and reduced temperature, ($T/T_c$) of 1.25 and 1.4 may be appropriate to delimit the Unsafe Zone/Gray Zone and Gray Zone/Safe zone. In addition, the specific volume and kinematic viscosity show asymptotic behavior at high SC pressures that can have important implications in the transport of hydrocarbons and natural gas. Moreover, the critical temperature, cricondentherm, and anomalous region of natural gas can be moved to lower temperatures by adding one or more modifier gases with low $T_c$, e.g., methane, nitrogen, and argon; or, higher using gases with high $T_c$ such as ethane, propane, and carbon dioxide. The pipelines carrying SNG, with $T_c$-modifications if needed, can therefore pass through polar, tropical, arid, and desert-like conditions.

## 1. Introduction

Efforts are being made to develop pipelines to transport natural gas at very high pressures, in the dense phase, i.e., above cricondenbar ($P_{cr}$). Katz and King described the dense phase, in 1973, as a state where (a) fluid is in a single phase with properties somewhere between those of a gas and a liquid, (b) is relatively incompressible, and (c) can expand or contract with the change in temperature. Later, King (1991, 1992) proposed the possibility of pipelines operating at near-ground temperatures and ultra-high pressures above 15 MPa. He followed his early works with the study on operating characteristics of buried natural gas pipelines in the permafrost regions. Pressures up to 42 MPa were considered with the goal to develop arctic pipelines (King et al., 2002). Another initial work on the dense phase pipelines of large diameter was reported by Mazurek and Anderson (1994). These pioneering studies were generally focused on the concept of transport of natural gas at very high pressures together with the design considerations for those pipelines. However, these authors did not analyze the details of unique fluid behavior at pressures that fall into the dense phase.

Botros (2002), possibly for the first time, discussed the five states of fluid in the operation of a pipeline: (i) liquid ($T < T_c$, $P < P_c$), (ii) chilled liquid ($T < T_c$, $P > P_c$), (iii) two-phase liquid-vapor, (iv) gas ($T > T_{cr}$, $P < P_{cr}$), and (v) dense phase ($T > T_c$, $P > P_{cr}$), where $T_{cr}$ is the cricondentherm. Campbell (2012), on his blog PetroSkills, has been discussing, for several years, the features of low-pressure versus high-pressure and dense phase natural gas transport. Through this blog, Moshfeghian (2009) first reported the dense phase properties of methane $-120$ °C $< T < -60$ °C, $P < 6$ MPa. Later, he considered the natural gas of a select composition for $-100$ °C $\leq T \leq 125$ °C, $P \leq 17$ MPa (Moshfeghian, 2010). Indeed, these pressures and temperatures ranged from liquid to

* Corresponding author.
*E-mail address:* vish.prasad@unt.edu (V. Prasad).

https://doi.org/10.1016/j.jgsce.2023.205072
Received 12 February 2023; Received in revised form 22 May 2023; Accepted 12 July 2023
Available online 25 July 2023

dense phase conditions. Moshfeghian's data could be useful when the state of the gas in a pipeline varied from liquid to liquid-vapor, and then to dense phase. Again, no attention was given to the anomalous behavior of the gas that was bound to occur in the critical region, from subcritical liquid to supercritical fluid.

Interestingly, in spite of the research on dense phase natural gas pipelines being initiated in 1970s, its implementation has taken a long time and is still in very early stages. Following are some of the projects where dense phase is either being used or has been proposed. Worldwide, Asgard field, located in the central area of the Norwegian Sea, is considered the first to have used dense phase transport of natural gas via a submarine pipeline. The pipeline has a length of about 440 miles with a diameter of 1 m. The Offshore Associated Gas project (OAG Project) in the United Arab Emirates also makes use of the dense phase. In this case, the gas is compressed, dehydrated, and transported through a 30" diameter pipe from production facilities in Das Island to the processing facilities in Habshan.

Nord Stream 1 (NS1), the longest subsea pipeline in the world, brings natural gas from Russia to Germany, 1167 km (Nord Stream, 2023). The inlet pressure in NS1 is reported to be close to 22 MPa (Beaubouef, 2011). However, to the authors' knowledge no scientific and engineering details of NS1 have been reported in the literature. An analysis by Moshfeghian et al. (2022) shows that this pipeline might be transporting natural gas in the dense phase at a mass flow rate of 647.7 kg/s. With the success of NS1, Nord Stream 2, a 1200 km-long offshore pipeline, is being constructed to connect Europe to the world's largest reserves in Northern Russia. However, NS2 has been put on hold because of the Russia-Ukraine war.

The use of high-pressure pipelines has also been proposed as a solution to the transport and production in hostile territories and low temperatures of the Arctic region. The main pilot project is All Alaska LNG, which will transfer enriched natural gas through a high-pressure, small-diameter pipeline from Prudhoe Bay to Cook Inlet (Baker, 2005). In addition, a proposal for Colombian Caribbean Sea, and the Tumaco and Chocó Offshore basins in the waters of the Colombian Pacific Ocean is in the works (Vargas-Vera et al., 2020).

Recently, Zivdar and Abofarakh (2021) have reported a simulation of both normal and dense phase transmission of natural gas via Iran's fourth national pipeline, without furnishing any evidence/data on whether this pipeline uses the dense phase or not. Also, the scope of simulation is very limited and does not provide much information on the property variations and flow behavior even though the pressure and temperature range considered by these authors fall right into the anomalous state.

Indeed, the previous authors by thinking of high pressures, $P > 5$ MPa, were contemplating the supercritical (SC) conditions without addressing the complexities of the SC fluids, particularly in the critical region. Note that, to avoid dew formation (phase change to liquid), the temperature of the natural gas under dense phase must be above $T_{cr}$ which is generally greater than $T_c$ in the case of natural gas, see Fig. 1 in Botros (2002) and Fig. 7 here. It is evident that there is a need to fully understand the dense phase of natural gas.

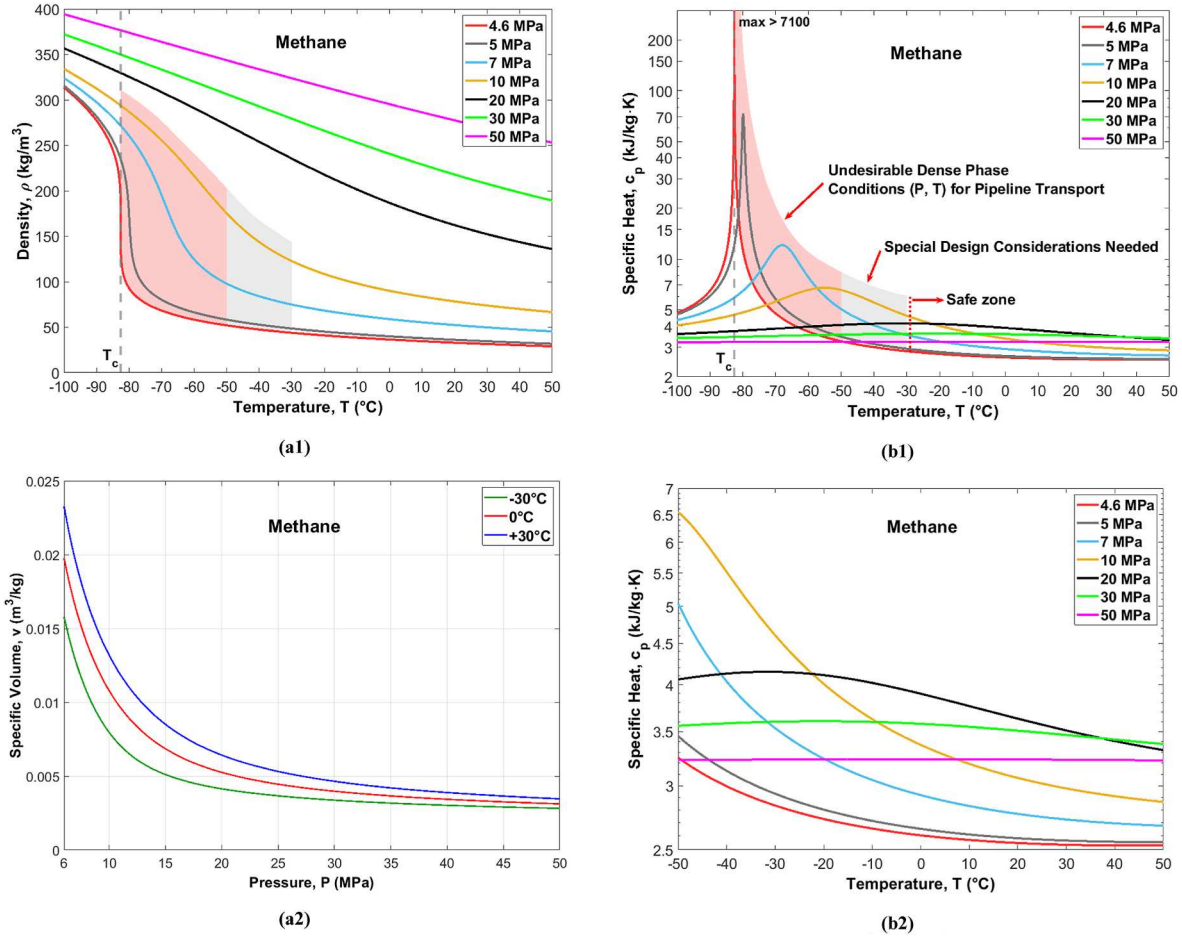


**Fig. 1.** Thermophysical Properties of methane (C1) at and above critical condition ($P_c = 4.60$ MPa, $T_c = -82.59$ °C): (a1) density, (a2) specific volume, (b1) isobaric specific heat, (b2) isobaric specific heat at high temperatures, (c1) dynamic viscosity, (c2) kinematic viscosity and (d) thermal conductivity, $k$. Light red and gray areas represent the zones of (i) undesirable dense phase conditions and (ii) special design considerations needed, respectively. Right to the Gray Zone is the Safe Zone for methane transport.

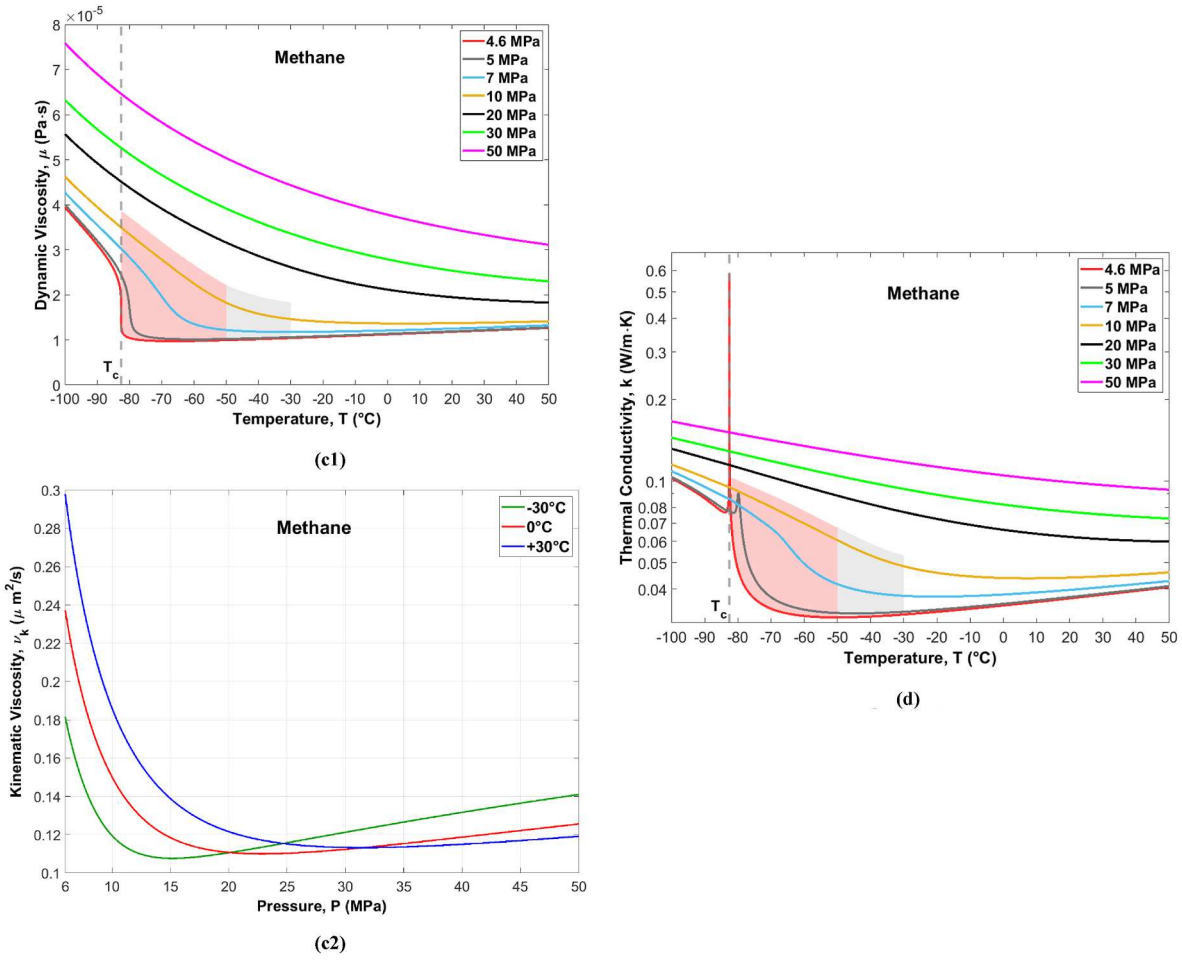


**Fig. 1.** (*continued*).

When the fluid approaches its critical point a major difficulty/challenge arises because of the existence of anomalous state in the vicinity of the critical point, on both subcritical and supercritical sides (Prasad et al., 2022a). Indeed, the initial belief that beyond the critical point the liquid and vapor are indistinguishable, has already been belied. It is now well established that the supercritical state consists of two parts: SC "liquid-like" (SCLL) and SC "gas-like" (SCGL). SCLL and SCGL belong to the anomalous state which is characterized by large scale variations in thermophysical properties, including inversions, flow and thermal instabilities/oscillations, and deteriorated heat transfer; see Pioro (2014), Imre et al. (2015, 2019), Han (2011), and Prasad et al. (2022a) for reviews on this topic.

Historically, as far back as in Benedict et al. (1940) had presented an empirical equation for isothermal variation of density with pressure, for hydrocarbons and their mixtures in the gaseous and liquid states. They considered pressures up to 30 MPa and temperatures up to 100 °C. Their modifications to the Beattie-Bridgeman equation provided more accuracy in the prediction of properties at high densities. Viscosity predictions of pure light hydrocarbons were later made by Eakin et al. (1947) using the Sutherland equation. The predictions agreed well with the observed data, within 4.4% except for the densities that were within 10% of the critical density. As we know now, the SC region immediately after the critical point is the anomalous region where the density variation could be quite large.

Younglove and Ely (1987) followed the Benedict's work and presented mathematical relations from which thermophysical and transport properties could be obtained for methane, ethane, propane, isobutene, and n-butane. Later, Friend et al. (1989) examined the quality of these correlations for methane in different regions of the phase diagram, against the experimental data from liquid to supercritical state, 92 K $< T <$ 623 K and 0.1 MPa $< P <$ 1000 MPa. Their goal was to improve accuracy, particularly in the extended critical region. They also reported divergence near the critical point for ethane, propane, butane, and carbon dioxide.

Setzmann and Wagner (1991) developed a new equation of state (EOS) for Helmholtz energy of methane and established correlations to represent better thermodynamic properties from melting temperature to 625 K and pressures up to 1000 MPa. The behavior of methane under SC conditions from 10 to 17 MPa was also investigated by Ricci et al. (2016), both experimentally and numerically using a 3D model. They provided the plots for density, specific heat, viscosity, and thermal conductivity up to 500 K which showed that the fluid around the critical point experienced significant variations in their properties.

A reference EOS with tabulated data for ethane, for pressures up to 900 MP, was presented by Bücker and Wagner (1991). Similarly, Friend et al. (1991) presented correlations for thermal conductivity ($90 < T <$ 600 K, $P <$ 70 MPa), and viscosity ($90 < T <$ 500 K, $P <$ 60 MPa) of ethane. On the other hand, Marsh et al. (2002) reported the experimental data on thermal conductivity of propane in a similar range of $P$ and $T$. Conducting an experimental investigation of transcritical methane, Votta et al. (2016) found that when the pressure was close to the critical value, the flow behavior and heat transfer were significantly affected. Some other notable works on hydrocarbons in the critical and supercritical regions are by Etter and Kay (1961), Hough and Stegemeier (1961), Moosavi and Abareshi (2012), and Grieves and Thodos (1962). The pseudo-critical region, also referred to as the Widom region, for

methane where the peaks of its various properties, e.g., $c_p$, $\beta$, and $\kappa$, lie on a *P-T* diagram, was presented by Imre et al., in 2019.

The supercritical properties of hydrocarbon fluids (n-$C_{10}H_{22}$ and n-$C_7H_{16}$) using a cubic EOS was evaluated by Li et al. (2017). They also provided the plots for density, heat capacity, viscosity and thermal conductivity as well as the NIST data for n-$C_{10}H_{22}$ and n-$C_7H_{16}$, for 300–800 K. A crossover description of transport properties, such as thermal conductivity and diffusivity for hydrocarbons near and around the critical point, was presented by Kaghazchi and Behnejad (2022). Wide-ranging correlations for thermodynamic properties of methane-ethane systems in the general region of critical point using analytic Schmidt-Wagner EOS were presented by Friend and Ely (1992). Cota and Thodos (1962), on the other hand, experimentally investigated the critical temperatures and pressures of hydrocarbon mixtures.

Excellent reviews of the progress made over the years to estimate or predict the thermophysical properties of fluids have been presented by Ahmed (2007), Mokhatab et al. (2019), and Elliott et al., (2023). Accurate values of thermophysical properties of hydrocarbons, mixture of hydrocarbons, and natural gas of various compositions can now be obtained from NIST models, REFPROP (Elliott et al., 2023).

Although the above works demonstrate excellent efforts to investigate and predict the properties of supercritical hydrocarbons and their mixtures, they do not analyze systematically the conditions under which the anomalous behavior (a) may exist, (b) the supercritical pressures and temperatures at which anomalies may disappear, and (c) the conditions beyond which the SC hydrocarbons and natural gas would show monotonic/gradual changes in its properties. Such states need to be identified since (c) is the region of invaluable significance to long distance, high mass flow rate transport of natural gases via pipelines passing through varying thermal conditions. This is one of the major objectives of the present research.

We then reveal that the dense phase as measured by its pressure above cricondenbar cannot guarantee that a mixture of gases, e.g., natural gas with various hydrocarbons and non-hydrocarbons as its constituents, will be devoid of thermophysical property-related complexities. This is because the cricondenbar and cricondentherm, both lie within the anomalous region. We show that the pipeline pressure being above cricondenbar from inlet to exit may be a necessary condition but not the sufficient condition for gas to be in a single phase. Therefore, it is critical that the SC thermophysical properties as well as the anomalous behavior are well characterized and the dense phase vis-à-vis anomalous state in the SC region are well understood. Then only we can prescribe the best pressure and temperature conditions for SC pipeline transport, including the dense phase conditions.

Our goal is then to use this information to delimit (a) the supercritical region, which is safe for the pipeline transport and (b) the region which should be avoided. The gases considered are: hydrocarbons (methane, ethane, and propane), mixtures of hydrocarbons and non-hydrocarbons, and natural gases. In addition, we demonstrate that it is possible to move the anomalous region as well as the Safe Zone to lower or higher temperatures by adding one or more modifier gases. A companion paper (Prasad et al., 2023) and a patent application (Prasad et al., 2022c) then present the distances (thousands of kilometers) to which supercritical natural gas (SNG) can be transported without recompression, as long as the "Safe Zone" (as determined here) is maintained from the inlet to exit, as well as how this distance varies with major flow parameters.

## 2. Behavior of supercritical hydrocarbons

As we know, all fluids exhibit large-scale variations in thermophysical properties near their critical points (CP) and this behavior continues far beyond the CP, in the supercritical region. However, the sharpness in changes as well as the peak values decrease as the SC pressure and/or temperature increase. Ultimately, the properties exhibit monotonic behavior at high SC pressures and temperatures. This anomalous behavior in the supercritical region close to CP, also referred to as the pseudo-critical region, is highly complex (Pioro, 2014; Imre et al., 2019; Prasad et al., 2022a). Note that the anomalous state extends well into the subcritical liquid (below the critical pressure and temperature) and therefore a gas moving from the state of liquid to dense phase/supercritical state during the transit, via a pipeline, would experience a large region of $P < P_c$ and $T < T_c$ to $P > P_c$ and $T > T_c$ as the anomalous state (Prasad et al., 2022a).

For the present study, it is important to consider first the behavior of hydrocarbons as a single fluid. Obviously, methane (C1) is the best choice for this purpose since it constitutes the dominant part (70–95%) of the natural gas; ethane (C2) and propane (C3) are considered next. To demonstrate the effect of adding a gas with much higher critical temperature to that of methane, the mixture of methane and ethane is considered as the Gas Mixture #1 (0.85 C1 + 0.15 C2). Gas Mixture #2 (0.8128 C1 + 0.0482 C2 + 0.004 C3 + 0.135 $N_2$) then shows the effect of adding nitrogen, a gas with much lower critical temperature. Finally, we examine the mixtures of various hydrocarbons, nitrogen, and carbon dioxide as Natural Gas A, B, and C, which represent the average/approximate compositions of gases from the US/Canada, West Asia, and North Sea, respectively (Table 1).

### 2.1. Supercritical methane (C1)

Thermophysical properties of methane – density, $\rho$, specific heat, $c_p$, dynamic viscosity, $\mu$, and thermal conductivity, $k$, obtained using NIST REFPROP V.10.0 (Lemmon et al., 2018), are presented in Fig. 1 (a)–(d) for pressure, $P = 4.6$ ($P_c$), 5, 7, 10, 20, 30, and 50 MPa and $-100\ ^\circ C < T < 50\ ^\circ C$ ($T_c = -82.586\ ^\circ C$, 190.564 K). Also, presented are the derived properties, heat capacity, $C_p$ ($= \rho \cdot c_p$), isobaric coefficient of volumetric expansion, $\beta$, and isothermal compressibility, $\kappa$, in Fig. 2(a), (b), and (c), respectively. The range of pressure and temperature considered in the case of methane as well as all other gases in Table 1 are shown in Table 2.

In Fig. 1(a1), (c1), and (d), $\rho$, $\mu$, and $k$, show substantial drops in their values near the critical point. On the other hand, $c_p$ in Fig. 1(b1) and $C_p$, $\beta$, and $\kappa$ in Fig. 2(a)–(c), first increase with temperature, achieve peak values, and then decrease to much lower values, the peaks being highest at CP. Indeed, the peaks of $c_p$, $C_p$, $\beta$, and $\kappa$ go to extremely high values. However, as the pressure increases beyond the critical point, $P_c$, the behavior of sharp variations is weakened, and at high SC pressures, they vanish, leading to almost monotonic trends. For example, isobaric lines for $c_p$, for pressures of 20 MPa and higher, show very smooth trends (Fig. 1b1 and 1b2), without any large variations and inversions, beyond $-20\ ^\circ C$. So do the lines for 4.6 and 5 MPa.

Fig. 1(b1) and 1(b2) show another anomaly in specific heat, i.e., $c_p$ at higher pressures is lower than that at lower pressures, e.g., $c_p$ at 20 MPa $> c_p$ at 30 MPa $> c_p$ at 50 MPa for $T < 40\ ^\circ C$. This can have important implications on heat transfer. It is therefore important that we consider the combined effect of $\rho$ and $c_p$ via $C_p$ (Fig. 2(a)) since the density and specific heat have very different behaviors in the SC region. Fig. 2(a) shows that $C_p$ decreases monotonically with $P$ at $T > -30\ ^\circ C$ although the rate of change is smaller at higher pressures than at lower pressures. In addition, there is no inversion in its values with increasing pressure, i.e., $C_p$ continuously increases with pressure when $T > -30\ ^\circ C$. The bottom line is that in the case of SC transport where pressure and temperature both may change, it is important that the thermal effects are carefully analyzed in designing the SNG pipelines.

The effect of $P$ and $T$ on volumetric expansion, $\beta$, is shown in Fig. 2 (b), which is very similar to that shown by $c_p$. While the monotonic behavior at high pressure and high temperature is again true, the value of $\beta$ may change in a complex manner in this region; see $T > -30\ ^\circ C$. Another parameter important to SC gas transport is isothermal compressibility, $\kappa$ (Fig. 2(c)), which decreases with increasing pressure and decreasing temperature, at $P > 15$ MPa. However, near the critical point, the change in $\kappa$ is again complex. Indeed, Fig. 2(c) undoubtedly exhibits that the fluid is not incompressible in the SC regime (or the

**Table 1**
Critical points of hydrocarbons and non-hydrocarbons considered here; compositions of gas mixtures and properties together with parameter for Eqs. (2) and (3), ω (Lemmon et al., 2018).

| Components | Mol. Wt, M g/mol | $P_c$, MPa | $T_c$, °C | $T_c$, K | ω | Gas Mix. # 1 | Gas Mix. #2 | Nat. Gas A | Nat. Gas B | Nat. Gas C |
|---|---|---|---|---|---|---|---|---|---|---|
| $N_2$ (Nitrogen) | 28 | 3.39 | −146.96 | 126.1 | 0.040 | | 13.50 | 0.50 | 1.62 | 0.700 |
| $CO_2$ (Carbon Dioxide) | 44.01 | 7.38 | 30.98 | 304.2 | 0.228 | | | 0.30 | 0.70 | 2.222 |
| C1 ($CH_4$, Methane) | 16.043 | 4.60 | −82.59 | 190.564 | 0.011 | 85 | 81.28 | 94.73 | 94.90 | 89.160 |
| C2 ($C_2H_6$, Ethane) | 30.1 | 4.88 | 32.18 | 305.33 | 0.099 | 15 | 4.82 | 4.20 | 2.50 | 7.350 |
| C3 ($C_3H_8$, Propane) | 44.1 | 4.25 | 92.68 | 365.86 | 0.152 | | 0.40 | 0.20 | 0.20 | 0.510 |
| i-C4 ($C_4H_{10}$, i-Butane) | 58.124 | 3.65 | 134.66 | 407.81 | 0.177 | | | 0.02 | 0.03 | 0.030 |
| n-C4 ($C_4H_{10}$, n-Butane | 58.124 | 3.80 | 151.98 | 423.13 | 0.199 | | | 0.02 | 0.03 | 0.024 |
| i-C5 ($C_5H_{12}$, i-Pentane) | 72.2 | 3.38 | 187.25 | 460.4 | 0.227 | | | 0.015 | 0.01 | 0.001 |
| n-C5 ($C_5H_{12}$, n-Pentane) | 72.2 | 3.37 | 196.60 | 469.5 | 0.249 | | | 0.015 | 0.01 | 0.003 |
| Total | | | | | | 100 | 100 | 100 | 100 | 100 |
| Critical Temperature $T_c$ (°C, K) | | | | | | −54.9, 218.25 | −76.75, 196.4 | −73.25, 199.9 | −77.15, 196.0 | −66.85, 206.3 |
| Cricondentherm $T_{cr}$ (°C, K) | | | | | | −49.35, 223.8 | −70, 203.15 | −66.90, 206.25 | −70.92, 202.23 | −58.15, 215.0 |
| Critical Pressure $P_c$ (MPa) | | | | | | 6.181 | 5.921 | 5.23 | 5.04 | 5.612 |
| Cricondenbar $P_{cr}$ (MPa) | | | | | | 6.245 | 5.985 | 5.35 | 5.189 | 5.908 |

Average representative compositions: A – US/Canada, B – West Asia, C – North Sea.

dense phase) at least up to 30 MPa. However, the slope of the curve does decrease as the pressure increases. In addition, the effect of temperature on $\kappa$ is not straightforward; it may even diminish at high temperatures. In spite of the above complex behavior, the SC fluids do exhibit monotonic property variation at high pressures and/or high temperatures. This is clearly displayed in Fig. 1(b2) and in the plots for $\rho$, $\mu$, $k$, $C_p$, $\beta$, and $\kappa$, for $T > -30$ °C in Fig. 1(a) and (c), (d), and 2 (a-c).[1]

#### 2.1.1. Significant change in behavior at high pressures

To further examine the effects of pressure, we have presented the specific volume, $v$, and kinematic viscosity, $\nu_k$, with pressure in Fig. 1 (a2) and 1(c2), respectively. Evidently, the specific volume shows an asymptotic behavior with pressure, its slope decreases substantially and becomes quite small. That means at high pressures, P > 30 MPa, the specific volume, density, and isothermal compressibility will change very little with the pressure. Also, the lower the temperature, the earlier would be the asymptotic trend. That means the observation by Katz and King (1973) and Vargas-Vera et al. (2020) that a fluid in dense phase is relatively incompressible is only true at very high pressures, $P > 25$ MPa; this pressure has not been achieved in the dense phase pipelines thus far. Consequently, the higher the pressure, the smaller will be the change in volume, flow velocity, and Reynolds number for the given mass flow rate, $\dot{m}$, and diameter of the pipe, $D$.

On the other hand, Fig. 1(c2) for kinematic viscosity, $\nu_k$, does not show a clear asymptotic trend, but does exhibit significant reduction in its value with an increase in pressure up to 15 MPa, beyond which the effect of pressure becomes weak and that of temperature becomes somewhat complex. Between 20 MPa and 50 MPa, the kinematic viscosity changes by ~33% at −30 °C and almost negligible at 30 °C. As a result, for fixed $\dot{m}$ and $D$, the Reynolds number ($\mathrm{Re} \propto v/\nu_k$) and friction factor, $f$, will change very little at high pressures, $P > 20$ MPa, which has important implications in the pipeline transport.

### 2.2. Desirable conditions (safe zone) for pipeline transport of methane

We believe that the best conditions for pipeline transport of SC methane is, therefore, when the behavior is monotonic and the rate of change of properties with pressure and temperature is not large. This assures that the fluid is outside the anomalous region and no flow oscillations and thermal instabilities would occur. Indeed, it is reasonable to assume that in the case of methane, $T > -30$ °C may be a safe zone for pressure from 5 to 50 MPa, or higher (see Figs. 1 and 2, particularly 1a2, 1b2, and 1c2). This is fortuitous since in most cases of gas transport, temperature below −30 °C may not be encountered, the exceptions being the very cold regions and arctics.

The temperature range of $-50$ °C $< T < -30$ °C is a region where the rate of change of properties is somewhat larger at lower pressures (see the lines for 10, 7, 5, and 4.6 MPa in Fig. 1b2), and therefore will require careful design of the pipelines. Evidently, a pipeline system with gas pressure of 10 MPa or lower at any location during the transit should not be designed for temperatures below −50 °C, since there would be property inversions. It is to be noted that the change in heat capacity, $C_p$, which accounts for the simultaneous changes in both density and specific heat (Fig. 2(a)), can affect the local temperature severely and create serious instabilities in the pipeline. The regions for undesirable conditions and where special design considerations would be needed for SC methane transport are shown with light red and gray colors in Fig. 1(a1, b1, c1, and d) and 2 (a, b). These zones are somewhat extended beyond the uppermost isobaric lines to account for uncertainties in the equations of state and model predictions.

Interestingly, as the temperature increases the behavior of methane even at lower pressures becomes smooth and normal. This provides another major advantage in the case of SC transport, i.e., if the gas exits in a region of $T \geq -30$ °C, irrespective of the inlet temperature (Fig. 1b2), there would be no cause for worries. We therefore believe that $P \geq 5$ MPa and $T \geq -30$ °C is the "Safe Zone" (SZ) for pipeline transport of supercritical methane whereas $5 = P \leq 10$ MPa and $-50$ °C $\leq T \leq -30$ °C is the "Gray Area" that may require special considerations (see also Section 4.4). *Note that even though the "Safe Zone" and "Gray Area" are shown on property plots, the conclusions are drawn for state conditions in terms of the pressure and temperature (P, T). No flow and thermal instabilities would be expected in the Safe Zone.*

### 2.3. Supercritical ethane (C2) and propane (C3)

As shown in Table 1, both the molecular weight, $M$, and critical temperature, $T_c$, of ethane (C2) are higher than that of methane (C1). Similarly, $M$ and $T_c$ of propane (C3) are larger than that of both ethane and methane. One can therefore conclude that the critical temperature, $T_c$ increases as the C-content of the hydrocarbon increases. However, the critical pressures of methane, ethane, and propane (4.60, 4.88, and 4.25 MPa) do not change much. Evidently, the trend of $P_c$ is not consistent with the C-content of hydrocarbons.

Graphically the density and specific heat of ethane and propane in

[1] Since the specific heat generally exhibits the full extent of anomalous region, only $c_p$ plots are presented for other gases and their mixtures.

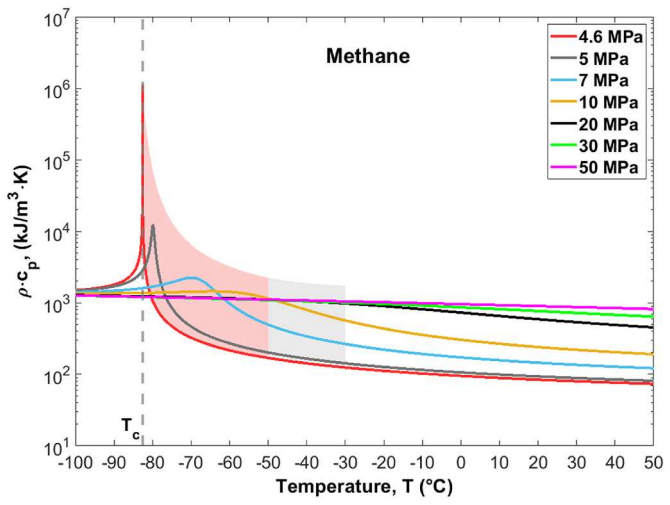


(a)

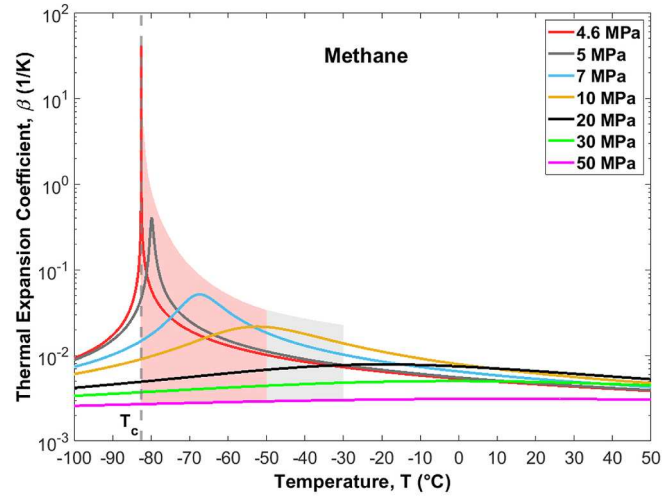


(b)

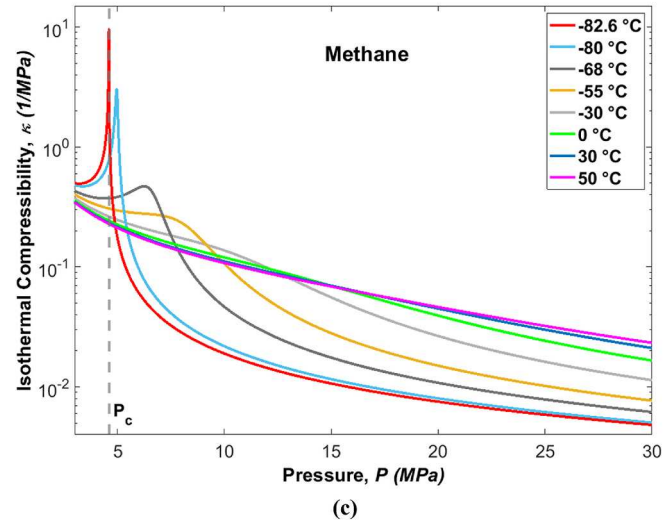


(c)

**Fig. 2.** (a) Heat capacity, $C_p$ (= $\rho \cdot c_p$), (b) isobaric coefficient of volumetric expansion, $\beta$, and (c) isothermal compressibility, $\kappa$, of methane at and above critical point.

Fig. 3(a–b) and 4(a-b) exhibit very similar behavior as shown by methane in Fig. 1(a1, b1) though they do differ in values and slopes of the isobaric lines. However, because of the critical temperature (see Table 1) being very different, the anomalous regions move far away from each other in terms of temperature. Clearly, this has important implications in terms of the supercritical transport of these gases. Indeed, the safe zone for methane, $P > 5$ MPa and $T > -30$ °C changes to $P > 5$ MPa and $T > 75$ °C for ethane, and to $P > 5$ MPa and $T > 150$ °C for propane. That means the flexibility of supercritical methane being transported at sub-zero or near-ambient temperature is not available with ethane and propane. Both of these gases will require to be heated at much above ambient temperature and maintained at higher temperatures if they are to be transported under SC conditions.

## 3. Methodology for calculations of mixture properties

There are several different equations of state available in the literature, including SRK, Peng-Robinson (PR), BWRS, AGA-8, GERG-88, GERG-2004; GERG-2008 to evaluate the thermodynamic properties of natural gas as a mixture (Ahmed, 2007; Helgaker, 2013; Mokhatab et al., 2019). Chaczykowski (2009) investigated the sensitivity of the gas pipeline flow model to the selection of EOS for SRK, BWRS, AGA-8 and GERG 88, for on-shore distribution network. The inlet pressure considered was only up to 7.4 MPa. The transient model by Chaczykowski (2009) was used by Helgaker (2013) to simulate the dynamics of offshore natural gas pipelines with the inlet pressure up to 18–20 MPa. Helgaker (2013) has also investigated the influence of the thermodynamic EOSs, including PR and GERG-2004 EOSs, on flow predictions. Noticeable divergence among various models were only observed at high pressures, $P > 10$ MPa. Even for $P > 10$ MPa, PR and GERG04 predictions are in the middle of the other model predictions.

The PR EOS also allows accurate predictions of the phase-behavior of mixtures of nonpolar systems encountered in the gas industry (Ahmed, 2007; Mokhatab et al., 2019). It has been incorporated into the two-phase model for Eulerian large-eddy simulations (LES) of liquid-fuel injection and mixing at high pressures (Matheis and Hickel, 2018). These authors have stated that the incorporation of the PR EOS model can represent the coexistence of supercritical states and multi-component sub-critical two-phase states via a homogeneous mixture approach. This is a desirable characteristic for modeling in the vicinity of the critical point. Given that, the liquid-like and gas-like molecules can coexist in the Widom delta/region, which is part of the anomalous phase (Ha et al., 2018), it is prudent to use the PR EOS for present modeling. This is justified by many other factors, such as the simplicity and flexibility of use and widespread industrial applications. In addition, the delimitation of the Safe Zone and Gray Area for methane (Section 2.2), has already indicated that the pressure for these zones in the case of natural gas will be below 10 MPa.

The Peng-Robinson cubic equation of state for a pure component is given as (Peng and Robinson, 1976):

$$P = \frac{RT}{v - b_i} - \frac{a_i \alpha_i}{v^2 + 2b_i v - b_i^2} \tag{1}$$

where $R$ is the universal gas constant, subscript $i$ represents the $i$th pure element in the mixture, and $a_i$ and $b_i$ are the corresponding constants related to its critical pressure ($P_{c,i}$) and critical temperature ($T_{c,i}$),

$$a_i = \Omega_a \frac{RT_{c,i}^2}{P_{c,i}} \quad b_i = \Omega_b \frac{RT_{c,i}}{P_{c,i}} \quad \text{with } \Omega_a = 0.45724 \; \Omega_b = 0.07780 \tag{2}$$

The temperature-dependent function that is related to the acentric factor, $\omega_i$, of the $i$th pure substance, is given by,

$$\alpha_i = \left[1 + \left(0.37464 + 1.54226\omega_i - 0.26992\omega_i^2\right)\left(1 - \sqrt{T/T_{c,i}}\right)\right]^2. \tag{3}$$

The equation of state for a pure compound is extended to the natural

**Table 2**
Range of pressure and temperature for the data presented here..

| Gas | Methane C1 | Ethane C2 | Propane, C3 | Mixture Gas #1 | Mixture Gas #2 | Natural Gas A | Natural Gas B | Natural Gas C |
|---|---|---|---|---|---|---|---|---|
| *P*, MPa | 4.6, 50[a] | 4.88, 50 | 4.25, 50 | 6.18, 50 | 5.92, 50 | 5.23, 50 | 5.04, 50 | 5.61, 50 |
| *T*, °C | −100, 50[a] | 0, 100 | 50, 200 | 100, 100 | −100, 100 | −100, 50 | −100, 100 | −100, 100 |

[a] The first number in each cell represents the lowest values of *P* or *T* and the second numbers the highest, for the data presented here. Thermophysical properties of all pure hydrocarbons and non-hydrocarbons are obtained using REFPROP (Lemmon et al., 2018) while that of the mixtures and natural gas are predicted using the PR EOS model.

gas mixture by the concept of a one-fluid mixture (Poling et al., 2000). It is assumed that for a fixed composition, the mixture properties and their variations with temperature and pressure can be described like a pure compound with adjusted parameters, $(a\alpha)_m$ and $b_m$ based on the composition of the mixture (Peng and Robinson, 1976),

$$P = \frac{RT}{v - b_m} - \frac{(a\alpha)_m}{v^2 + 2b_m v - b_m^2} \tag{4}$$

The following classical mixing rules have been adopted in the present model (Soave, 1972):

$$(a\alpha)_m = \sum_i \sum_j \left[ z_i z_j \sqrt{a_i a_j \alpha_i \alpha_j} \left(1 - k_{ij}\right) \right] \tag{5}$$

$$b_m = \sum_i (z_i b_i) \tag{6}$$

where $z_i$ is the mole fraction of $i$th pure element in the natural gas mixture. The parameter $k_{ij}$ in Eq. (5) is an empirically determined correction factor (called the *binary interaction coefficient*) designed to characterize any binary system formed by components $i$ and $j$ in the hydrocarbon mixture. These binary interaction coefficients are used to model the intermolecular interaction through empirical adjustment of the $(a\alpha)_m$ term as represented mathematically by Eq. (5). They are dependent on the difference in molecular size of the components in a binary system and are characterized by the following properties (1) hydrocarbon components with the same molecular weight have a binary interaction coefficient of zero; and (2) the binary interaction coefficient matrix is symmetric: $k_{i,j} = k_{j,i}$. Studies (Privat and Jaubert, 2011; Ahmed, 2007) have shown that $k_{ij}$ may also depend on the temperature and models were proposed to estimate them at different temperatures. To simplify the calculations, all $k_{ij}$ are treated as constants and are listed in Table 3 (Ahmed, 2007).

### 3.1. Other properties

For any given pressure, *P* and temperature, *T*, the density of fluid mixture $\rho$ can be found by solving the cubic equation of state, Eq. (4). The thermal expansion coefficient, $\beta$, of the mixture can be calculated by

$$\beta = \frac{1}{v}\left(\frac{\partial v}{\partial T}\right)_P = -\frac{1}{v}\frac{(\partial P/\partial T)_v}{(\partial P/\partial v)_T} \tag{7}$$

and the isothermal compressibility, κ, of the mixture is

$$\kappa = -\frac{1}{v}\left(\frac{\partial v}{\partial P}\right)_T = -\frac{1}{v(\partial P/\partial v)_T} \tag{8}$$

where,

$$\left(\frac{\partial P}{\partial T}\right)_\rho = \left(\frac{\partial P}{\partial T}\right)_v = \frac{R}{v - b_m} - \frac{(a\alpha)_m'}{v^2 + 2b_m v - b_m^2}$$
$$\left(\frac{\partial P}{\partial v}\right)_T = -\frac{RT}{(v - b_m)^2} + \frac{2(a\alpha)_m (v + b_m)}{\left(v^2 + 2b_m v - b_m^2\right)^2} \tag{9}$$

The specific heat at constant volume, $c_v$, of the mixture can also be calculated from the equation of state,

$$c_v = c_p^0(T) - R - \frac{(a\alpha)_m'' T}{2\sqrt{2} b_m} \ln\left|\frac{v + \left(1 - \sqrt{2}\right) b_m}{v + \left(1 + \sqrt{2}\right) b_m}\right| \tag{10}$$

where $c_p^0(T)$ is the specific heat at constant pressure of ideal gas mixture at the given temperature *T*, and can be obtained by weighted average of specific heat, $c_{p,i}^0$, of the individual ideal gas pure element *i*,

$$c_p^0(T) = \sum_i \left[ z_i c_{p,i}^0(T) \right] \tag{11}$$

The ideal gas specific heat ($c_{p,i}^0$) of relevant pure element *i* is estimated from the following polynomial equation (Passut and Danner, 1972; Mangold et al., 2019),

$$\frac{c_{p,i}^o}{R} = d_{1,i} + d_{2,i} T + d_{3,i} T^2 + d_{4,i} T^3 + d_{5,i} T^4 \tag{12}$$

with $d_{j,i}$ ($j$ = 1, 2, …5) as the fitting constants of experimental data.

The specific heat at constant pressure, $c_p$, of the mixture is then calculated by the following equation,

$$c_p - c_v = -T\frac{(\partial p/\partial T)_v^2}{(\partial p/\partial v)_T} \tag{13}$$

For any given composition of the mixture, $z_i$, the vapor-liquid equilibrium (VLE) can be determined to provide a phase envelope for the mixture, following the method discussed by Ahmed (2007). The phase envelope is made of the dew-point pressure ($P_d$) at which an infinitesimal amount of liquid first appears from a saturated vapor for a given temperature, and the bubble-point pressure ($P_b$) at which the first bubble of gas is formed from the saturated liquid mixture at a given temperature. The dew-point pressure curve meets the bubble-point pressure curve at the critical point ($P_c$, $T_c$) of the mixture. From these two curves, we can also identify the cricondenbar, $P_{cr}$ (the highest pressure on the phase envelope), and the cricondentherm, $T_{cr}$ (the highest temperature on the dew-point pressure curve).

Predictions using the above equations have been made for the range of pressure and temperature as noted in Table 2. Since we are focused on stable, monotonic behavior of the gas mixtures (away from the critical point), the selection of highest pressure to 50 MPa is based on the hydrocarbons and their mixtures exhibiting nice, smooth trends all the way from the subcritical to supercritical states (Figs. 1–4 and 8–10). This implies that the trend will not change at $P > 50$ MPa. The selection of lowest and highest temperatures in these figures are driven by our motivation to demonstrate the range of anomalous states and the stable SC regime with the rate of change in properties as a function of *P* and/or *T* being small. A flow chart for present calculations and data analysis is shown in Fig. 5.

### 3.2. Error, sensitivity, and validation of PR model

The original and later modified PR EOS models have been employed throughout the petroleum industry and have produced acceptable data for many practical applications (Ahmed, 2007; Lopez-Echeverry et al., 2017; Mokhatab et al., 2019). Significant deviations of the predictions from the real situation have been observed, particularly in the region near the critical point (Lopez-Echeverry et al., 2017). For example,

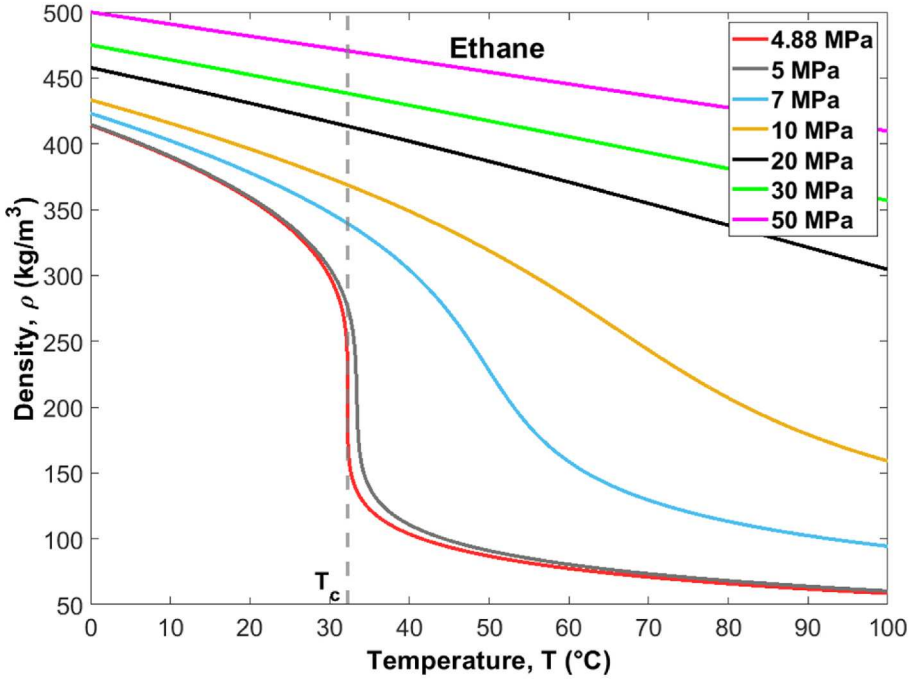


(a)

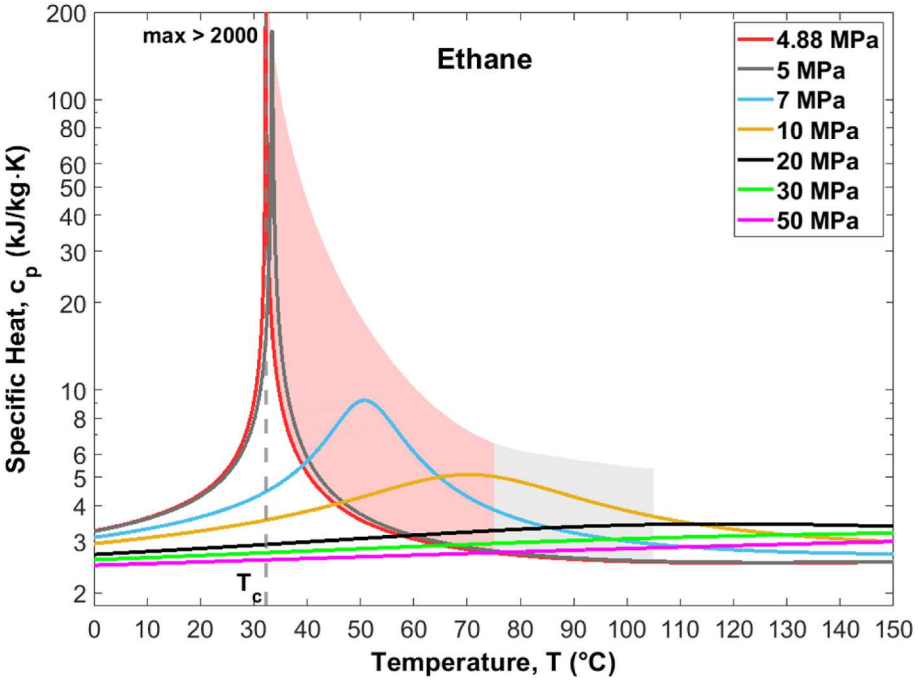


(b)

**Fig. 3.** Thermophysical properties of ethane at and above critical condition ($P_c$ = 4.88 MPa, $T_c$ = 32.18 °C): (a) density and (b) isobaric specific heat.

Faradonbeh et al. (2013) conducted a comparative study of eight cubic EOSs (including SRK and PR, YL, VPT, etc.) for the predictions of thermodynamic properties of alkanes and found that the all EOSs (i) were able to show the heat capacity maxima with varying degrees of accuracy at temperatures, $T > T_c$, (ii) all EOSs performed closely with the exception of the VPT EOS which highly underestimated the results, and (iii) in the SC region, the best results were obtained by YL and PR EOSs for compounds up to C5 with an error of 3% that is relevant to the present study.

Similarly, through a comparative study of eleven EOSs in predicting the thermodynamic properties of hydrogen, Nasrifar (2010), found that all EOSs in all families were accurate in predicting the constant pressure

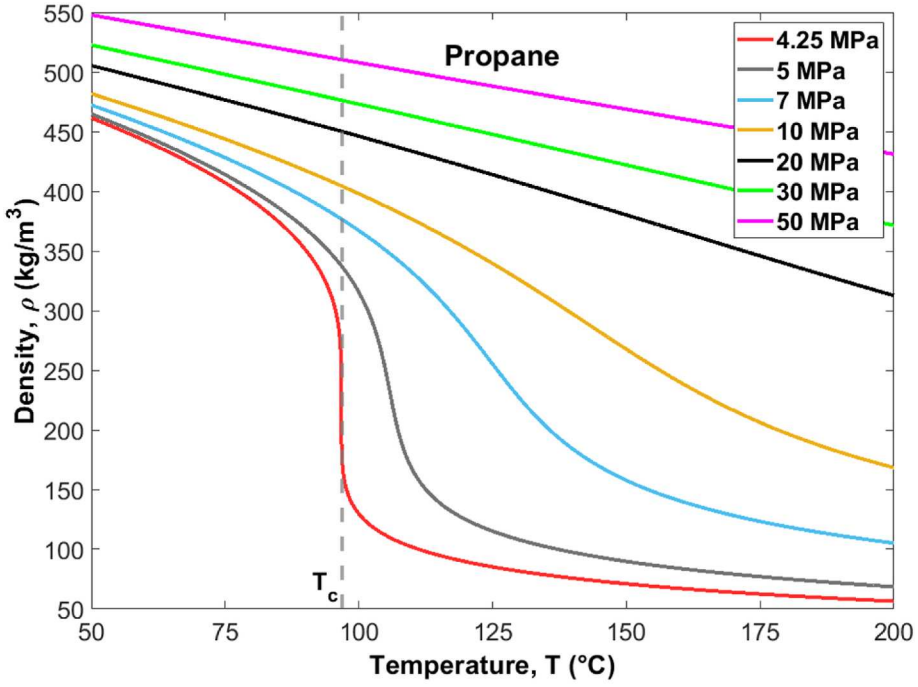


(a)

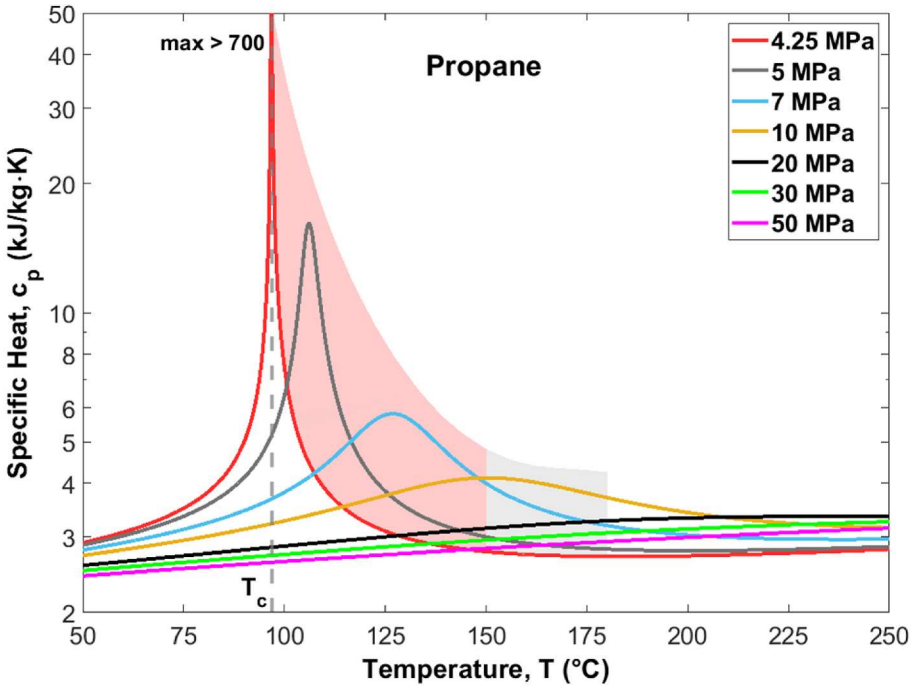


(b)

**Fig. 4.** Thermophysical Properties of Propane at and above critical condition ($P_c$ = 4.25 MPa, $T_c$ = 92.68 °C): (a) density and (b) isobaric specific heat.

heat capacities of hydrogen. However, the most accurate EOSs were the PT, RKS and PR EOSs. Recently, Perez et al. (2017) conducted a comparative study of the vapor-liquid equilibrium (more relevant the present gases in the Widom region), and density modeling of mixtures related to carbon capture and storage with the SRK, PR, PC-SAFT and SAFT-VR Mie EOSs for industrial uses. They found that despite the differences among these EOSs, they are accurate enough for ($P$, $v$, $T$) modeling of fluids related to carbon capture. In general, the SAFT-VR Mie EOS better predicts the VLE with an average deviation of 13.3% compared to the experimental data for equilibrium pressure, followed

**Table 3**
Binary interaction coefficient, $k_{ij}$, used with the Peng-Robinson EOS (adapted from Ahmed, 2007).

| | $CO_2$ | $N_2$ | $C_1$ | $C_2$ | $C_3$ | i-$C_4$ | n-$C_4$ | i-$C_5$ | n-$C_5$ |
|---|---|---|---|---|---|---|---|---|---|
| **$CO_2$** | 0 | 0 | 0.105 | 0.130 | 0.125 | 0.120 | 0.115 | 0.115 | 0.115 |
| **$N_2$** | | 0 | 0.025 | 0.010 | 0.090 | 0.095 | 0.095 | 0.100 | 0.100 |
| **$C_1$** | | | 0 | 0.005 | 0.010 | 0.035 | 0.025 | 0.050 | 0.030 |
| **$C_2$** | | | | 0 | 0.005 | 0.005 | 0.010 | 0.020 | 0.020 |
| **$C_3$** | | | | | 0 | 0.000 | 0.000 | 0.015 | 0.015 |
| **i-$C_4$** | | | | | | 0 | 0.005 | 0.005 | 0.005 |
| **n-$C_4$** | | | | | | | 0 | 0.005 | 0.005 |
| **i-$C_5$** | | | | | | | | 0 | 0.000 |
| **n-$C_5$** | | | | | | | | | 0 |

Note that $k_{ij} = k_{ji}$.

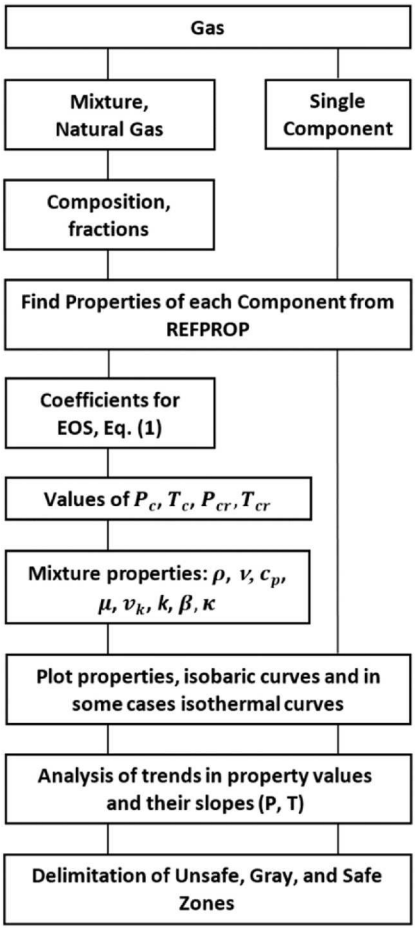


**Fig. 5.** Flow Chart for calculation of the properties of gas and gas mixtures.

by the CEOS, with 13.7% for the SRK and 14.2% for the PR EOSs.

In addition, Kunz and Wagner (2012) have compared the predicted phase envelopes of several natural gas mixtures by the PR EOS model with that by a more accurate GERG2008 model. Though the correct shape of the phase enveloped are predicted by both models, the predicted cricondenbars and cricondentherm by the PR EOS model deviated from the experimental data more than that by GERG 2008. Similar trends have also been observed recently by Zhang et al. (2020) who have experimentally studied more than two dozens of natural gas mixtures.

These studies indicate that the PR EOS model can provide acceptable predictions of the thermophysical properties of normal gas mixtures including the natural gases of small molecular weights, particularly, in the pressure and temperature ranges away from the critical point, as in our case. Indeed, a rather higher uncertainty of the phase envelope predicted by the PR EOS should not affect the general observations and conclusions made in our study since our focus is on delimiting the gray area and safe zone. As shown in Table 4 and Section 5.1, these zones start at $T_r$ of 1.25 and 1.4 respectively, with $P_r$ being 1.15 for both of them.

**Table 4**
Temperature at which the Gray and Safe Zones start.

| Gas | $T_c$ K | $T_{gray}$ | $T_{safe}$ |
|---|---|---|---|
| Methane | 190.56 | −50 °C | −30 °C |
| | | 223 K | 243 K |
| | | **1.171**[a] | **1.276** |
| Ethane | 305.33 | 75 °C | 105 °C |
| | | 348 K | 378 K |
| | | **1.140** | **1.238** |
| Propane | 365.83 | 150 °C | 180 °C |
| | | 423 K | 453 K |
| | | **1.157** | **1.239** |
| Mixture Gas #1 | 218.25 | 0 °C | 30 °C |
| | | 273 K | 303 K |
| | | **1.252** | **1.389** |
| Mixture Gas #2 | 196.40 | −30 °C | −10 °C |
| | | 243 K | 263 K |
| | | **1.238** | **1.340** |
| Natural Gas A | 199.90 | −50 °C | −30 °C |
| | | 223 K | 243 K |
| | | **1.116** | **1.216** |
| Natural Gas B | 196.00 | −35 °C | −10 °C |
| | | 238 K | 263 K |
| | | **1.215** | **1.343** |
| Natural Gas C | 206.30 | −15 °C | 5 °C |
| | | 258 K | 278 K |
| | | **1.251** | **1.348** |

[a] Numbers in bold are reduced temperatures, $T_r = T/T_c$, both temperatures in K.

Fig. 6(a) and (b) present the specific heat, $c_p$, and density, $\rho$, for Natural Gas A obtained using the present PR EOS model as well as the REFPROP (NIST), for $P = 10$ MPa and 30 MPa and $-100\ °C < T < 60\ °C$. As is evident, the agreement for $c_p$ is excellent at both the pressures and $T > -40\ °C$, and the variation at the peak for 10 MPa, $T \approx -53\ °C$ is the largest, ~10%. The density, $\rho$, also shows a very good agreement for both pressures at $T > -30\ °C$; the difference at −30 °C being about 7%. The difference then increases to ~8.5% at −50 °C. Our estimate is that in the Safe Zone, the error in using the PR model may not exceed 5% whereas it may increase up to 10% as the pressure moves towards the left side of the Gray Zone, $P = 6$ MPa and $T = -50\ °C$ (See Section 5.2 for the delimiting $P$ and $T$ for Gas A).

## 4. Characteristics of a gas mixture

### 4.1. Critical temperature and cricondentherm of gas mixtures

Fig. 7 demonstrates how the curves on phase diagram change with

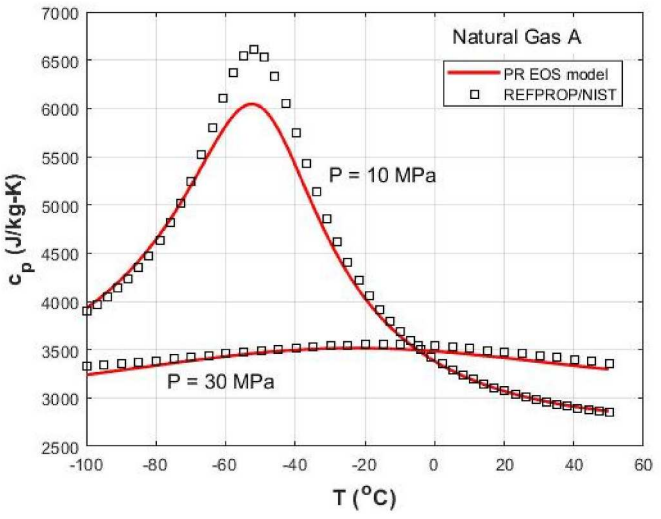


(a)

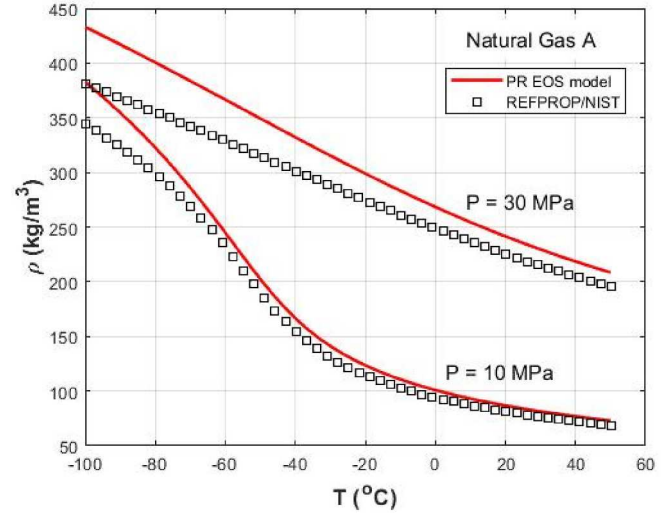


(b)

**Fig. 6.** (a) Specific heat and (b) density predictions using the present model compared with data obtained from REFPROP .

the fraction of the constituents of Mixture Gas #1 and 2 and Natural Gas A, B, and C. For example, as in Table 1 when 0.15 C2 (ethane) is added to C2 (methane), the critical temperature of the mixture (Gas #1) goes up since $T_c$ of ethane (C2) is much higher than that of the methane (C1). Similar effect of high C-content hydrocarbon was shown by Abd et al. (2021). On other hand, if 13.5% of $N_2$ with much lower $T_c$ is added to C1+C2+C3 (Gas #2), the $T_{c,mix}$ decreases significantly. On the other hand, in the case of Natural Gas A, B, and C, the critical temperature is found to increase because of the $T_c$'s of C2, C3, C4, and C5 are all higher than that of the methane (C1). Evidently, the critical temperature of a mixture has a simple relationship with $T_c$'s of its constituents and their fractions (Table 1 and Fig. 7).

On the contrary, the critical pressure of a mixture has a complex relationship with the $P_c$'s of its constituents and their fractions. For example, $P_c$ of the Mixture Gas #1 ($C_1$ and $C_2$) goes up compared to the $P_c$ of both the constituents; Mixture Gas #2 has a similar trend. Gases A, B, and C also show a similar behavior with respect to the hydrocarbons but they do not cross the $P_c$ of $CO_2$ (7.38 MPa) even when its fraction is above 2%. Furthermore, Fig. 7 and Table 1 exhibit that for the cases

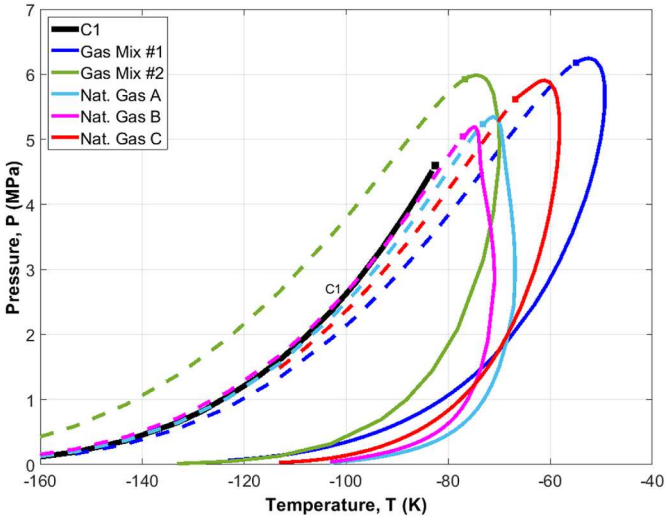


**Fig. 7.** Liquid-vapor line for Methane (C1); bubble point (dotted line) and dew point (full line) curves for Gas Mixtures #1 and 2 and Natural Gas A, B, and C; and critical points (square symbols). See Table 1 for chemical compositions of Gas Mixtures #1 and 2 and Natural Gas A, B, and C, and numerical values of critical pressure, $P_c$ and critical temperature, $T_c$, of mixtures and their constituents as well as the cricondenbar, $P_{cr}$, and cricondentherm, $T_{cr}$ of the mixtures.

considered here, both cricondenbar, $P_{cr}$, and cricondentherm, $T_{cr}$, of the mixtures are higher than their critical pressures, $P_c$, and critical temperatures, $T_c$, respectively.

### 4.2. Customized modifications in mixture properties

An important aspect of the results for Gas #1 and Gas #2 is that the critical temperature and cricondentherm of a mixture increase if a gas with higher critical temperature is added, e.g., Gas #1 -vs- C1 (Methane), and they decrease if a gas with lower critical temperature is added, Gas #2 -vs- C1 (Prasad et al., 2022b). This has many implications with respect to the transport of natural gas. For example, if the SNG is required to pass through very cold regions where the gas temperature may go below the desired temperature - based on the condition that its state must remain beyond the anomalous region, a higher percentage of methane may help. Nitrogen ($T_c$ = −146.96 °C) and Argon ($T_c$ = −122.46 °C) are the other gases that can be used for the purpose of bringing down the critical temperature and cricondentherm. Argon, has an additional advantage of being non-reacting and non-corroding (Prasad et al., 2022a). Note that as $T_c$ goes down, the anomalous region also shifts to the left on the temperature line, compare Fig. 8(b) with Fig. 2(b).

However, if the surrounding conditions demand higher critical temperature as well as higher cricondentherm, it can be achieved by adding any other hydrocarbons than methane or one or more non-hydrocarbons, like $CO_2$, with higher $T_c$. This will move the anomalous region to higher temperatures (to the right). Addition of higher C-content hydrocarbon(s) has another advantage of enriching the gas and increasing its calorific value. This may be beneficial when the natural gas enriched with high carbon-content hydrocarbons such as ethane and/or propane are to be transported within the tropical and warmer regions.

Furthermore, Fig. 8(a) and (b) for specific heat of Mixture Gas #1 and #2 demonstrate that the general behavior with respect to pressure and temperature beyond the critical point remain the same as seen for C1, C2, and C3 in Figs. 1–4 except that the peaks have moved to the right because of the higher $T_c$ of ethane in Fig. 8(a) and to the left because of the lower $T_c$ of nitrogen Fig. 8(b).

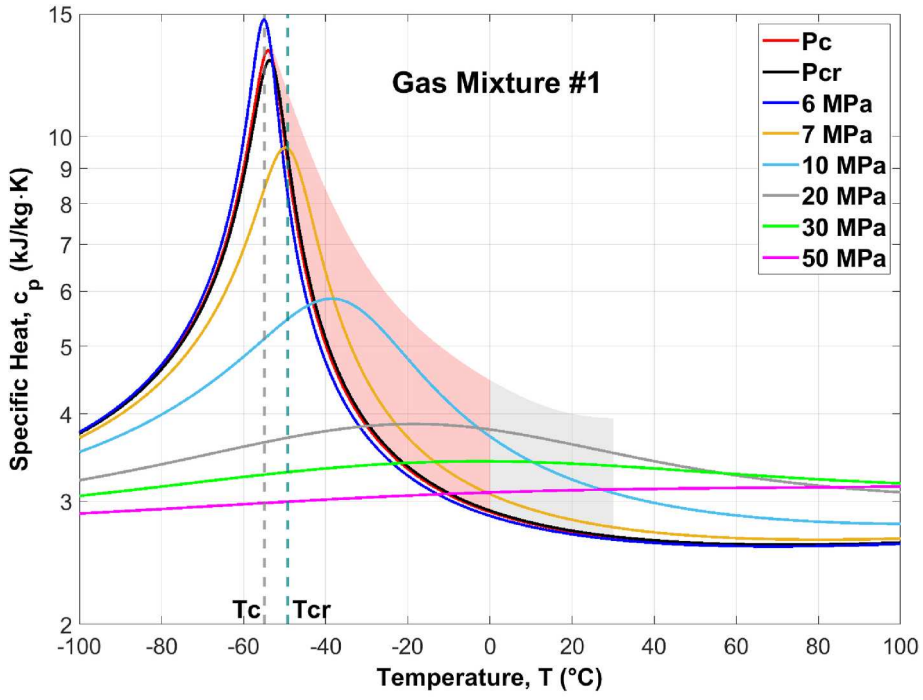


(a)

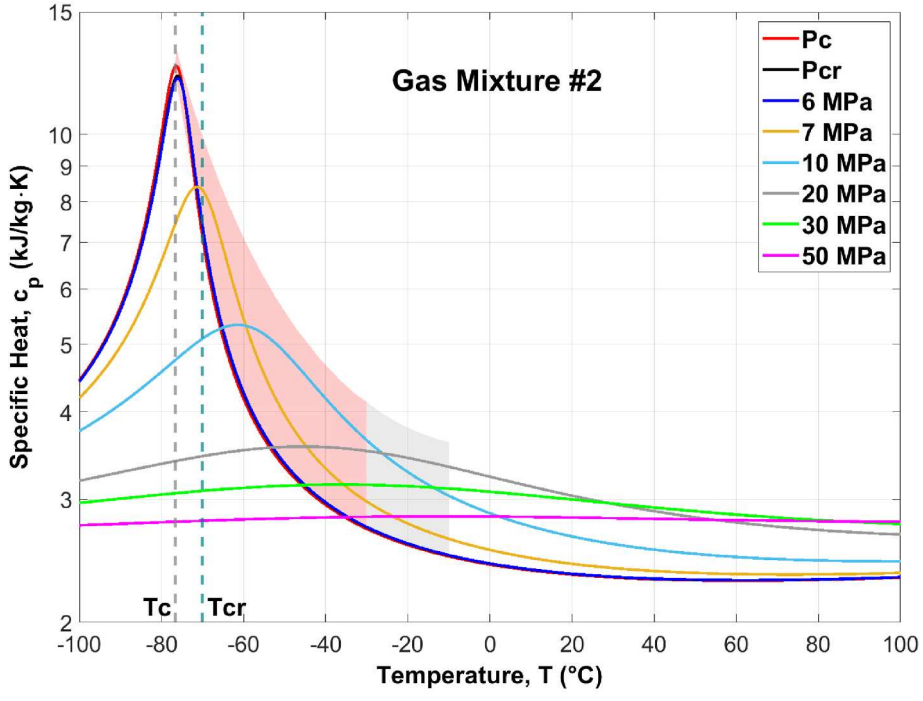


(b)

**Fig. 8.** Isobaric specific heat, $c_p$, for (a) Gas Mixture #1 (85 C1 + 15 C2) ($P_{cr} = 6.245$ MPa and $T_{cr} = -49.35$ °C), and (b) Gas Mixture #2 (81.28 C1 + 4.82 C2 + 0.4 C3 + 13.5 $N_2$) ($P_{cr} = 5.985$ MPa and $T_{cr} = -70$ °C), see Table 1. Light red and gray areas represent the zones of (i) undesirable dense phase conditions and (ii) special design considerations needed, respectively. Right to Gray Zone is the Safe Zone for pipeline transport.

## 5. Characteristics of natural gas

### 5.1. Thermophysical properties of natural gas

Figs. 9 and 10 present the results for Natural Gas A and Natural Gas B and C, respectively. As is evident from the comparison among Fig. 9(a–f) for $\rho$, $c_p$, $\mu$, $C_p$, $\beta$, and $\kappa$, and Fig. 1(a1), (b1), and (c1) and Fig. 2(a), (b), and (c), the general behavior of all of the properties of Gas A is similar to what is observed in the case of methane. Indeed, other gases, B and C also support this observation for all properties. Note that only $c_p$ curves are shown here for Gas B and C in Fig. 10(a) and (b), respectively. The differences are only in their values. In all of these cases, there exist an

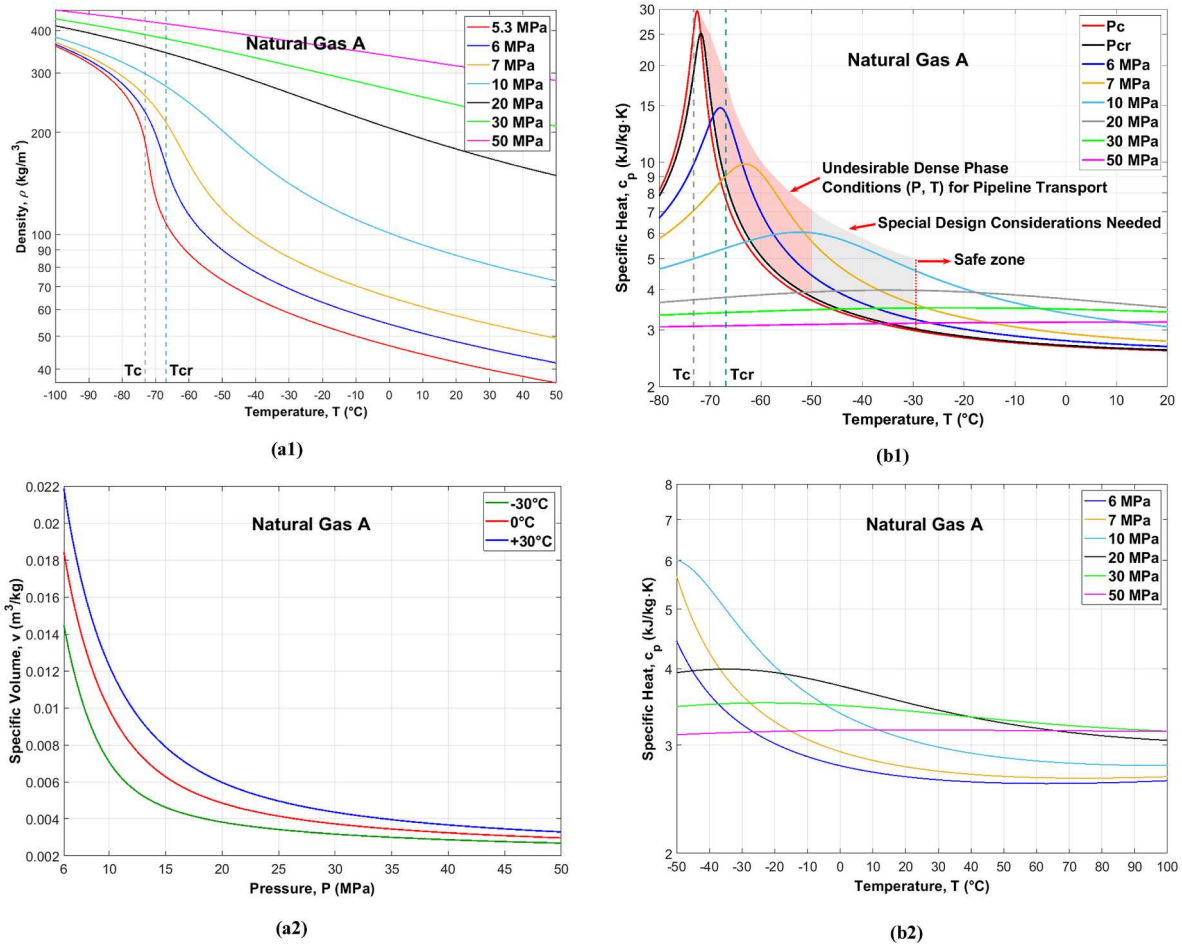


**Fig. 9.** (a1) Density, (a2) specific volume, (b1) specific heat, (b2) specific heat at high temperatures, (c1) dynamic viscosity, (c2) kinematic viscosity, (d) heat capacity, $C_p$, (e) isobaric coefficient of volumetric expansion, and (f) isothermal compressibility for Natural Gas A ($P_{cr} = 5.35$ MPa and $T_{cr} = -66.90$ °C). Light red and gray areas represent the zones of (i) undesirable dense phase conditions and (ii) special design considerations needed, respectively. Right to Gray Zone is the Safe Zone for the transport of natural Gas A Figure 9(b2).

anomalous region where properties vary sharply and inversions in $c_p$, $C_p$, $\beta$, and $\kappa$, occur as shown in Fig. 9(b), (d), (e), and (f), respectively.

Following observations regarding the thermophysical properties of natural gas can therefore be made from Fig. 9(a)–(f) for Gas A:

(a) Fig. 9(a1) does not support a general statement that the density of natural gas in dense phase is closer to that of the liquid (Vargas-Vera et al., 2020), $\rho_{liquid} \approx 425$ kg/m$^3$ at 0.1 MPa and −165 °C. Indeed, the density varies substantially when $P > P_{cr}$ and $T > T_{cr}$ and this must be accounted for when the SNG flows from a high SC pressure to a low SC pressure.

(b) The density, $\rho$, at $P > 20$ MPa is a simple function of temperature, $T$ all the way from subcritical liquid to supercritical fluid states (Fig. 9a1).

(c) Isobaric specific heat, $c_p$, also has a simple relationship with temperature, $T$ at $P > 20$ MPa when $T > -10$ °C, but not with the pressure, $P$ (Fig. 9b1). However, $c_p$ increases monotonically with pressure at $T > 80$ °C ().

(d) Interestingly, Fig. 9(d) shows that the heat capacity, $C_p$, almost independent of pressure and temperature, at $P > 20$ MPa and $T < T_{cr}$ becomes almost a linear function of temperature at $P > 20$ MPa and $T >$ -25 °C. Moreover, the slope of $C_p$-$T$ line decreases with increasing pressure, $P$, which implies that the increase in $c_p$ with $P$ gets compensated by the decrease in $\rho$ at very high SC pressures and temperatures.

(e) Like methane, dynamic viscosity, $\mu$, decreases as the temperature increases, when the pressure is high but it increases with temperature when the pressure is low, $P \leq 10$ MPa (Fig. 9c1). Hence, the pressure loss will go down as SNG at high pressures moves from a cold region to a warm region, contrary to what would happen at low pressures.

(f) In addition, the general statement that the viscosity of natural gas in the dense phase is similar to that of the gas (Vargas-Vera et al., 2020) is not true, see 0.1 MPa gas line in Fig. 9(c1). Indeed, it varies significantly with the pressure and temperature.

(g) Natural gas is not incompressible in the SC regime (or the dense phase) contrary to the previous assumptions (Katz and King, 1973; Vargas-Vera et al., 2020) at P < 20 MPa (Fig. 9a1 and 9a2). For example, at 25 °C, the isothermal compressibility, $\kappa$, for 6 MPa is almost 10 times larger than at 30 MPa. Note that for a given pressure of 10 MPa, it increases by an order-of-magnitude from −100 °C (liquid) to 50 °C (SC fluid).

(h) Like methane, Natural gas A also shows the asymptotic behavior for specific volume with pressure, its slope decreases substantially and becomes small. That means at high pressures, P > 30 MPa, the specific volume, density, and isothermal compressibility will change very little with the pressure. In addition, the lower the temperature, the earlier would be the asymptotic trend.

(i) Also, like methane Natural Gas A exhibits significant reduction in its kinematic viscosity, $\nu_k$, with an increase in pressure up to 15

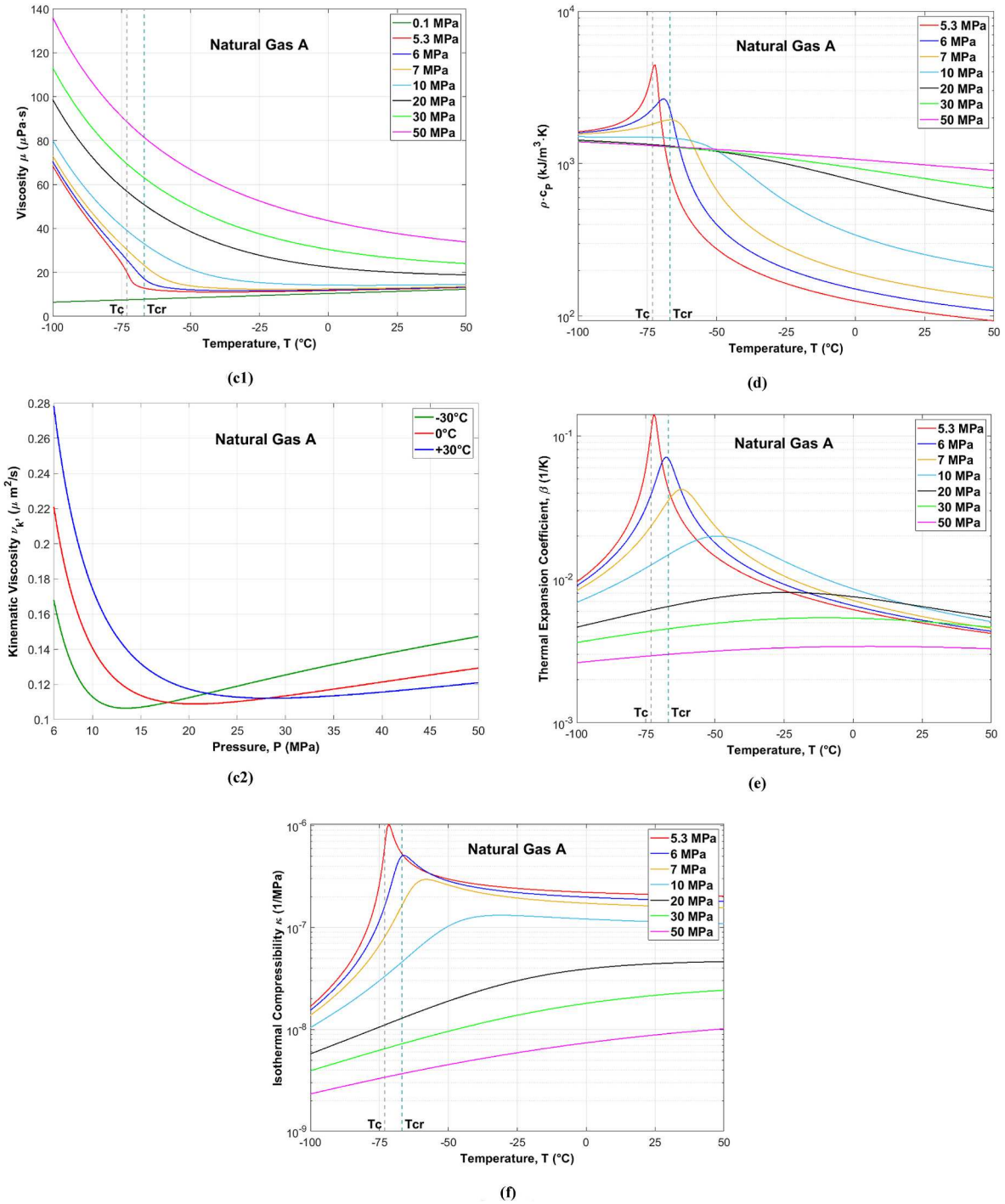


**Fig. 9.** (*continued*).

MPa, beyond which the effect of pressure becomes weak and that of the temperature becomes somewhat complex (Fig. 9c2).

(j) Between 20 MPa and 50 MPa, the change in kinematic viscosity is almost negligible, at 30 °C. Consequently, for fixed $\dot{m}$ and $D$, the Reynolds number (Re $\propto \nu/\nu_k$) and friction factor, $f$, for Gas A will change very little at high pressures, $P > 20$ MPa. This, again, has important implications in the pipeline transport.

(k) Note that the above observations will also be true for Natural Gas B and C although the pressure and temperature range as mentioned above may change, in particular the temperature.

In addition, an important conclusion from Figs. 9 and 10 for Gas A, B, and C is that the cricondentherm is always within the anomalous region and this region extends to somewhat higher temperatures than that of methane. For example, the lines for 6, 7, and 10 MPa, in Fig. 9(b1) for Gas A ($T_{cr} = -66.90$ °C) do show inversions, and monotonic trends are established much later in terms of the temperature, after $T_c$ and $T_{cr}$. The line for 20 MPa shows a weaker trend and it can be concluded that at $P > 20$ MPa, the anomalous behavior of Gas A will be weaker. A similar trend is exhibited by Gas B (Fig. 10(a)). In the case of Gas C, the pressure required for non-anomalous behavior will be above 25 MPa (Fig. 9(b)).

It should also be noted that compared to methane (C1), the non-anomalous region is delayed in the case of Natural Gas A, B, and C because of the presence of high C-content hydrocarbons and $CO_2$ with

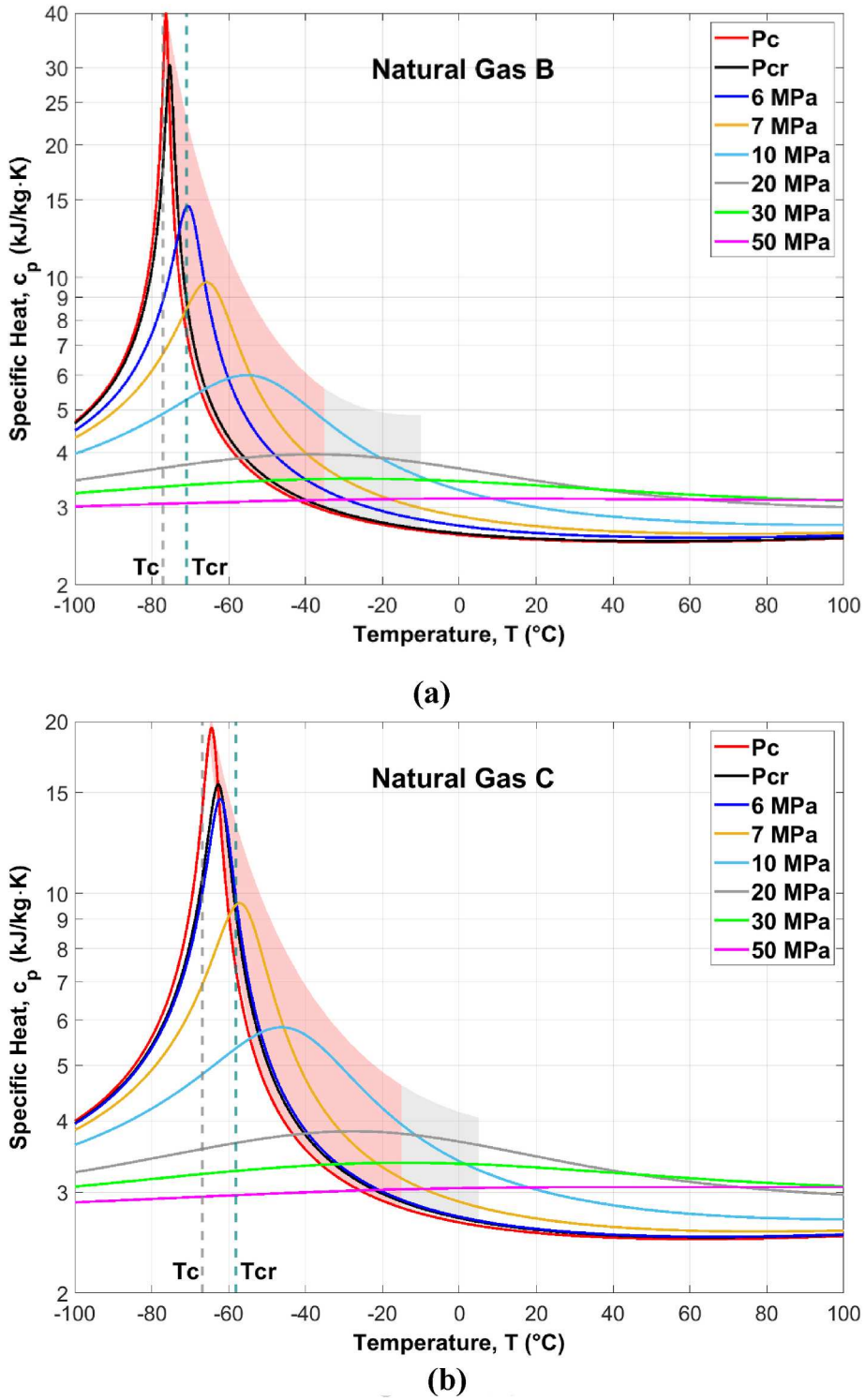


**Fig. 10.** Specific heat ($c_p$) for (a) Natural Gas B ($P_{cr} = 5.189$ MPa and $T_{cr} = -70.92$ °C), and (b) Natural Gas C ($P_{cr} = 5.908$ MPa and $T_{cr} = -58.15$ °C). Light red and gray areas represent the zones of (i) undesirable dense phase conditions and (ii) special design considerations needed, respectively. Right to Gray Zone is the Safe Zone for transport.

higher $T_{c's}$; this phenomenon was discussed in Section 4.2. However, the mixture can move to non-anomalous supercritical conditions, with property changes being gradual and smooth, at $P > P_c$ and $T > -10$ °C (Fig. 9b1, 10a, and 10 b). Temperature as low as $-30$ °C may be acceptable as long as the exit temperature of the gas is higher, e.g., $T > -10$ °C for $P = 6$ MPa. These effects are much more evident in Fig. 11(a) where $c_p$ for methane and Gas A, B, and C are compared. However, as the pressure and/or temperature increase the lines for three gases come closer and closer (Fig. 11a–d).

Indeed, there can be much more flexibility in designing SNG pipelines if the exit temperature is higher and the gas is delivered in a region with $T > 0$ °C. If the delivery is being made in a cold region, e.g., $T < 0$ °C, the design of pipelines would be somewhat complex. Fortuitously, the peaks of $c_p$, $C_p$, $\beta$, and $\kappa$ of Gas A (Fig. 9b1, d-f), as well as $c_p$ of Gas B

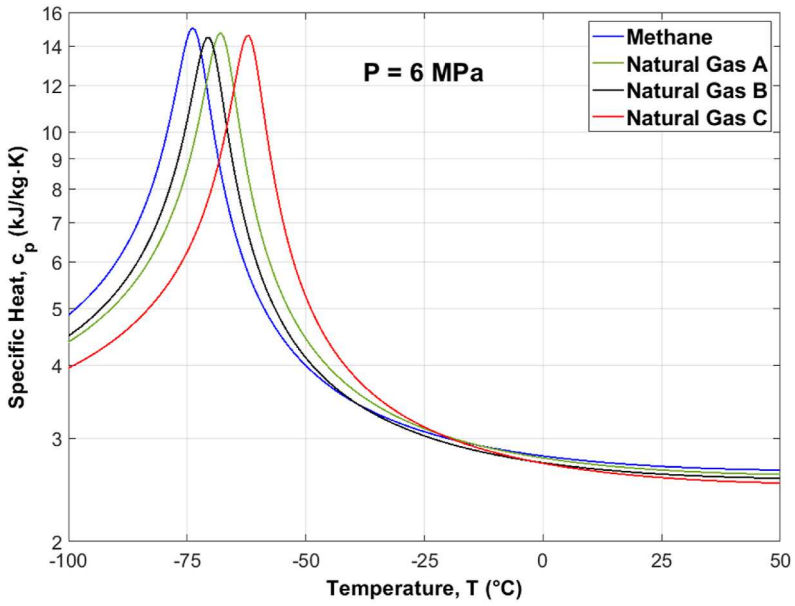


(a)

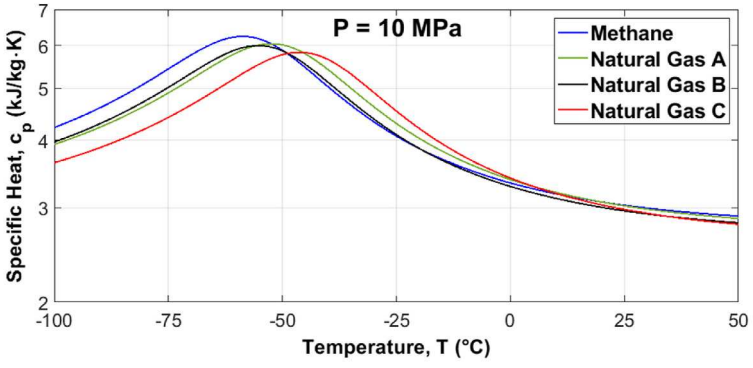


(b)

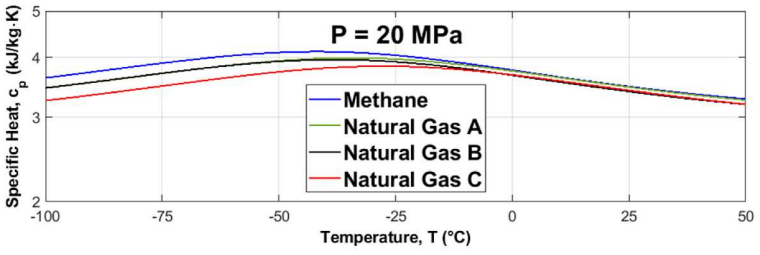


(c)

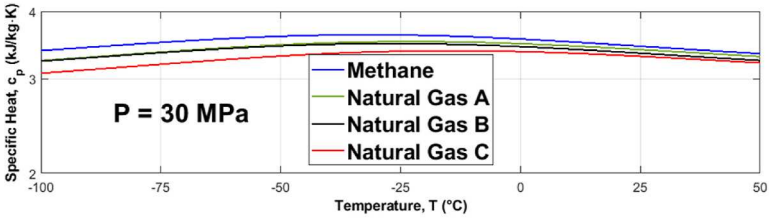


(d)

**Fig. 11.** Specific heat, $c_p$, for methane and Gas A, B, and C at (a) 6 MPa, (b) 10 MPa, (c) 20 MPa, and (d) 30 MPa.

and C all lie at $T < -40$ °C, that means the inversions in these properties would occur at temperatures below −40 °C. Careful design of the pipeline to account for large changes in properties but no inversions may allow the exit to occur at temperatures as low as −40 °C. As noted earlier, methane and/or nitrogen-rich gases can be delivered at much lower temperatures than the Gas A, B, and C considered here. Alternatively, it may be advantageous to add nitrogen or even argon, both of which are easily available.

### 5.2. Safe and gray zones for SNG transport

From the thermophysical properties of Gas A, B, and C as presented in Figs. 8–10 it can be concluded that $P > 6$ MPa and $T > -30$ °C is a safe zone (in terms of the physical state) for the pipeline transport of SNG since none of the properties will show large, unmanageable variations in their values and, of course, no inversions will take place. $P \geq 6$ MPa and $-50\ °C \geq T \geq -30$ °C, on the other hand will be a gray area that will require special considerations. The safe zone and gray area are shown only on the plot for $c_p$ (Fig. 9b1) and not repeated in the other Figures, 9 (a) and 9(c)–(f).

To develop some kind of correlations for the start of Gray and Safe zones for hydrocarbons and natural gas, the estimated temperatures delimiting the boundaries for all eight cases are presented in Table 4. Thermodynamically, it is more appropriate to consider the delimiting temperatures and pressures in terms of dimensionless reduced temperature, $T_r$, and pressure, $P_r$. In Table 4, $T_r$ for the start of Gray Zone varies from 1.140 to 1.252 and that for the Safe Zone from 1.216 to 1.389. Reduced temperature, $T_r$ of 1.25 may be therefore appropriate (conservative) to delimit the Gray Zone from Unsafe Zone. Similarly, $T_r$ of 1.4 separates the Safe zone from Gray Zone. For gases without significant heat transfer, reduced pressure, $P_r$ of 1.15-1.2 may be a good choice.

### 5.3. Applications of the present research

We believe, the natural gas pipeline industry would be the first to benefit from (i) the thermophysical property data based on the composition of the gas and flow conditions ($P$, $T$) presented here, (ii) the knowledge on anomalous behavior, and (iii) the conditions for safe transport of natural gas under supercritical conditions. Natural gas industry engaged in extraction and transportation from the distant onshore and offshore wells to processing facilities may benefit from the understanding of how the gas behaves in transcritical and supercritical states. So will be the industry engaged in transport to and from the natural gas storage. In addition, the behavior and phenomena presented here can provide much better understanding of high-pressure gas transport in other fields, for example, $CO_2$ transport for carbon capture and storage (CCS), transport of near-critical and supercritical gases in thermal power plants, fluid flow in supercritical heat exchangers, and so on.

### 5.4. Limitations and future work

The theoretical model adopted here for gas mixtures is based on the Peng-Robinson cubic equations of state, whose accuracy is a strong function of the applicability of the mixture theory to natural gases and reliability of the various coefficients used in the calculations. In addition, the delimiting conditions for gray and safe zones are estimated through visual observations and analysis of the change in values of the major properties and their gradients with pressure and temperature. However, this should not be a major concern in the design of natural gas pipelines since the industry always uses constraints conservatively.

With respect to future work, now that the major phenomena and general behavior are established and a foundation is built, an effort could be made to develop thermodynamics-based methodology to delimit the boundaries. It may also be possible to use molecular dynamics (MD) model to accomplish this task. In addition, it would be helpful if such methods can also delimit the boundaries where the anomalous regions stars in the subcritical (liquid/vapor) phase, $P < P_c$ and/or $T < T_c$, in three quadrants of the $P$-$T$ phase diagram. This can then reveal the phase complexities, the natural gas will encounter, when the phase transition takes place from liquid to SC fluid via the anomalous state while moving through a pipeline.

## 6. Concluding remarks

As demonstrated, cricondenbar, cricondentherm, and a part of the dense phase fall within the anomalous region where any small change in temperature and/or pressure can cause flow oscillations, thermal instabilities, and decreased heat transfer. Indeed, most of the assumptions about dense phase, such as incompressibility, density closer to that of the liquid, and viscosity closer to that of the gas, are questionable, for pressures at least up to 20 MPa, in the case of methane and natural gas. Most high-pressure pipeline systems currently do not exceed this pressure.

Like most fluids, hydrocarbons and their mixtures, including natural gas, exhibit monotonic and gradual variations in their properties at high SC pressures and/or temperatures, away from the anomalous states. Therefore, the most desirable conditions for the transport of SNG and other gas mixtures are: (a) above the critical pressure and critical temperature, (b) above the cricondenbar and cricondentherm (not applicable in the case of a single gas), and (c) beyond the anomalous state, throughout the transit from inlet to exit.

For SC methane, the Safe Zone in terms of pressure and temperature is, $P \geq 5$ MPa and $T > -30$ °C. On the other hand, $P \geq 5$ MPa and $-50\ °C > T > -30$ °C may be considered as gray area where the rate of change of properties is somewhat larger, particularly at the lower SC pressures. That means, special design considerations will be needed if there is any possibility of the gas experiencing the Gray Zone. For ethane, the safe and gray zones would be $P \geq 5.5$ MPa, $T > 105$ °C and $P \geq 5.5$ MPa and $75\ °C > T > 105$ °C, whereas for propane, the two zones would be $P \geq 5$ MPa, $T > 180$ °C and $P \geq 5$ MPa and $150\ °C > T > 180$ °C, respectively.

Based on the average compositions of natural gas from US/Canada, West Asia, and North Sea, $P \geq 6$ MPa and $T > -30$ °C may be considered as the Safe Zone for pipeline transport of SNG whereas $P \geq 6$ MPa and temperature, $-50\ °C < T < -30$ °C will be the Gray Zone. A conservative estimate of the start of Gray Zone may be $P_r \approx 1.15$ and $T_r \approx 1.25$ and that for the Safe Zone as $P_r \approx 1.15$ $T_r \approx 1.4$. If the composition of natural gas varies significantly from the three considered here, the methodology described in Section 3 can be used to determine the safe zone and gray area.

It is also discovered that the specific volume, density, and isothermal compressibility of hydrocarbons and natural gas have an asymptotic trend with respect to pressure and they become weak functions of pressure at high pressures, e.g., $P > 25$ or 30 MPa. Also, the lower the temperature, the earlier would be the asymptotic trend. This is the regime where the observations by Katz and King (1973) may apply.

In the case of pipeline transport, if the natural gas passes through a region where there is the possibility of gas temperature decreasing below the desired temperature, one or more modifier gases (hydrocarbons or non-hydrocarbons) with lower critical temperatures can be added. This would reduce the critical temperature and cricondentherm, and move the anomalous region to lower temperatures. However, if the anomalous region needs to be moved to higher temperatures, one or more modifier gases with higher $T_c$ can be added. Evidently, the SNG transport can allow the natural gas pipelines to pass through polar, tropical, arid, and desert-like conditions as well as through the land, underground, lakes, and ocean.

The behavior and phenomena observed here will also be true to other fluids, such as water, carbon dioxide, argon, nitrogen, oxygen, and their mixtures, under supercritical states.

## Funding

The first (LA) and third authors (VP) were partially supported by the US National Science Foundation NSF Award No. 2231393.

## Declaration of competing interest

The authors declare that they have no known competing financial interests or personal relationships that could have appeared to influence the work reported in this paper.

## Data availability

Data will be made available on request.

## Acronyms and Notations

*Symbols*

| | |
|---|---|
| $a_i$ | Coefficients of *i*th element in Peng-Robinson EOS, Eq. (1) |
| $b_i$ | Constants for *i*th element in Peng-Robinson EOS, Eq. (1) |
| C1 | Methane, $CH_4$ |
| C2 | Ethane, $C_2H_6$ |
| C3 | Propane, $C_3H_8$ |
| C4 | Butane, $C_4H_{10}$ |
| C5 | Pentane, $C_5H_{12}$ |
| $c_v$ | Specific heat at constant volume, J/kg • K |
| $c_p$ | Specific heat at constant pressure, J/kg • K |
| $C_p$ | Heat capacity at constant pressure ($\rho c_p$), J/m$^3$ • K |
| $D$ | Diameter, m |
| $f$ | Friction factor |
| $k$ | Binary coefficient in PR equation, Table (3) |
| $L$ | Length, m |
| $m_i$ | Coefficient of *i*th element in Eq. (3) |
| $\dot{m}$ | Mass flow rate, kg/s |
| $M$ | Molecular weight, g/mol |
| $P$ | Pressure, Pa, MPa |
| $P_{cr}$ | Cricondenbar, MPa |
| $R$ | Universal gas constant, J • K$^{-1}$ • mol$^{-1}$ |
| $Re$ | Reynolds number |
| $T$ | Temperature, °C, K |
| $T_{cr}$ | Cricondentherm, °C, K |
| $v$ | Specific volume, m$^3$/kg |
| $z_i$ | Mole fraction of *i*th element |

*Greek Symbols*

| | |
|---|---|
| $\alpha_i$ | Temperature-dependent function, Eq. (3) |
| $\beta$ | Isobaric coefficient of volumetric expansion, K$^{-1}$ |
| $\kappa$ | Isothermal compressibility, Pa$^{-1}$ |
| $\mu$ | Dynamic viscosity, N • s• m$^{-2}$ |
| $\nu_k$ | Kinematic Viscosity, m$^2$ • s$^{-1}$ |
| $\rho$ | Density, kg/m$^{-3}$ |
| ω | Accentric factor |
| Ω | Correlation constants, Eq. (2) |

*Subscript*

| | |
|---|---|
| a | Ambient/outside |
| b | Bubble-point |
| c | Value at critical point |
| d | Dew-point |
| cr | Value at criconden condition |
| i, j | Constituent of mixture |
| m | Based on the composition of the mixture, Eqs. (4)–(6) |
| mix | Mixture |
| P | Derivative at constant pressure |
| r | Reduced pressure, temperature |
| T | Derivative at constant temperature |
| w | Wall |
| $\rho$ | Derivative at constant density |

*Abbreviations*

| | |
|---|---|
| ARK | Aungier-Redlich-Kwong |
| EOS | Equation of state |
| GERG | European Gas Research Group |
| LNG | Liquefied natural gas |
| PC | Perturbed chain |
| PR | Peng-Robinson |
| RK | Redlich-Kwong |
| SAFT | Statistical associating fluid theory |
| SC | Supercritical |
| SRK | Soave-Redlich-Kwong |
| SNG | Supercritical natural gas |
| VLE | Vapor-liquid equilibrium |
| VR | Variable range |

## References


Abd, A.A., Naji, S.Z., Alwan, H.H., Othman, M.R., Tye, C.T., 2021. Impact of heavy hydrocarbon concentration on natural gas flow through transportation pipelines. IOP Conf. Ser. Mater. Sci. Eng. 1094, 012068 https://doi.org/10.1088/1757-899X/1094/1/012068.

Ahmed, T., 2007. Equations of State and PVT Analysis – Applications for Improved Reservoir Modeling, second ed. Gulf Publishing Company, Houston, Texas, pp. 378–409.

Baker, M., 2005. Transport of North Slope Natural Gas Tidewater. Alaska Natural Gas Development Authority.

Beaubouef, B., 2011. Nord stream completes the world's longest subsea pipeline. Offshore 30. http://www.offshore-mag.com/business-briefs/equipment/engineering/article/16755095/nord-stream-completes-worlds-longest-subsea-pipeline. (Accessed 16 January 2023).

Benedict, M., Webb, G.B., Rubin, L.C., 1940. An empirical equation for thermodynamic properties of light hydrocarbons and their mixtures I. Methane, ethane, propane and n-butane. J. Chem. Phys. 8, 334. https://doi.org/10.1063/1.1750658.

Botros, K.K., 2002. Performance of five equations of state for the prediction of VLE and densities of natural gas mixtures in the dense phase region. Chem. Eng. Commun. 189 (2), 151–172. https://doi.org/10.1080/00986440211837.

Bücker, D., Wagner, W., 1991. A reference equation of state for the thermodynamic properties of ethane for temperatures from the melting line to 675 K and pressures up to 900 MPa. J. Phys. Chem. Ref. Data 35, 205. https://doi.org/10.1063/1.1859286.

Campbell, J.M., 2012. Low Pressure versus High Pressure Dense Phase Natural Gas Pipeline Transportation. PetroSkills. http://www.jmcampbell.com/tip-of-the-month/2012/09/low-pressure-versus-high-pressure-dense-phase-natural-gas-pipeline-transportation/. (Accessed 9 January 2023).

Chaczykowski, M., 2009. Sensitivity of pipeline gas flow model to the selection of the equation of state. Chem. Eng. Res. Des. 87 (12), 1596–1603. https://doi.org/10.1016/j.cherd.2009.06.008.

Cota, H.M., Thodos, G., 1962. Critical temperature and critical pressures of hydrocarbon mixtures. Methane Ethane-n-Butane System. J. Chem. Eng. Data 7 (1), 62–65. https://doi.org/10.1021/je60012a018.

Eakin, B.E., Ellington, R.T., Aime, M., 1947. Predicting the Viscosity of Pure Light Hydrocarbons. Inst. of Gas Technology.

Elliott, J.R., Diky, V., Knotts IV, T.A., Wilding, W.V., 2023. The Properties of Gases and Liquids, sixth ed. McGraw Hill. ISBN: 978-1-26-011635-9.

Etter, D.O., Kay, W.B., 1961. Critical properties of mixtures of normal paraffin hydrocarbons. J. Chem. Eng. Data 6 (3), 409–414. https://doi.org/10.1021/je00103a026.

Faradonbeh, M.R., Abedi, J., Harding, T.G., 2013. Comparative study of eight cubic equations of state for predicting thermodynamic properties of alkanes. Can. J. Chem. Eng. 91 (1), 101–110. https://doi.org/10.1002/cjce.20682.

Friend, D.G., Ely, J., 1992. Thermodynamic properties of the methane-ethane system. Fluid Phase Equil. 79, 77–88. https://doi.org/10.1016/0378-3812(92)85121-N.

Friend, D.G., Ely, J.F., Ingham, H., 1989. Thermophysical properties of methane. J. Phys. Chem. Ref. Data 18, 583. https://doi.org/10.1063/1.555828.

Friend, D.G., Ingham, H., Fly, J.F., 1991. Thermophysical properties of ethane. J. Phys. Chem. Ref. Data 20, 275. https://doi.org/10.1063/1.555881.

Grieves, R.B., Thodos, G., 1962. The critical temperature of ternary hydrocarbon systems. Ind. Eng. Chem. Fund. 1 (1), 45–48. https://doi.org/10.1021/i160001a008.

Ha, M.Y., Yoon, T.J., Tlusty, T., Jho, Y., Lee, W.B., 2018. Widom delta of supercritical gas−liquid coexistence. J. Phys. Chem. Lett. 9 (7), 1734–1738. https://doi.org/10.1021/acs.jpclett.8b00430.

Han, S., 2011. Anomalous change in the dynamics of a supercritical fluid. Phys. Rev. E 84, 051204.

Helgaker, J.F., 2013. Modeling Transient Low in Long Distance Offshore Natural Gas Pipelines, Phil. Doctoral Thesis, Dept. Energy and Processes Eng. Norwegian Univ. of Science and Technology (NTNU), Trondheim, Norway.

Hough, E.W., Stegemeier, G.L., 1961. Correlation of surface and interfacial tension of light hydrocarbons in the critical region. Soc. Petrol. Eng. J. 1 (4), 259–263. https://doi.org/10.2118/197-PA.

Imre, A.R., Ramboz, C., Deiters, U., Kraska, T., 2015. Anomalous fluid properties of carbon dioxide in the supercritical region: application to geological $CO_2$ storage and related hazards. Environ. Earth Sci. 73 (8), 4373–4384. https://doi.org/10.1007/s12665-014-3716-5.

Imre, A.R., Groniewsky, A., Györke, G., Katona, A., Velmovszki, D., 2019. Anomalous properties of some fluids – with high relevance in energy engineering – in their pseudo-critical (Widom) region. Periodica Polytech., Chem. Eng. 63 (2), 276–285. https://doi.org/10.3311/PPch.12905.

Kaghazchi, S.R., Behnejad, H., 2022. Crossover description of transport properties for some hydrocarbons in the supercritical region. Chem. Phys. Lett. 792, 139394 https://doi.org/10.1016/j.cplett.2022.139394.

Katz, D.L., King, G.G., 1973. Dense Phase Transmission of Natural Gas. Energy Processing Canada.

King, G., 1991. Ultra-high pressure Arctic natural gas pipelines. In: Proceedings of Canadian Petroleum Association, Pipeline Conference, pp. 14–16. Calgary, Alberta Canada.

King, G., 1992. Ultra-high gas pressure pipelines offer advantages for Arctic service. Oil Gas J. 90, 79–84.

King, G., Kedge, C., Zhou, X., Matuszkiewicz, A., 2002. Superhigh dense phase Arctic pipelines increase reliability and reduce costs. In: Proceedings of iPC'02. 4th International Pipeline Conference, pp. 2002–27302.

Kunz, O., Wagner, W., 2012. The GERG-2008 wide-Range equation of state for natural gases and other mixtures: an expansion of GERG-2004. J. Chem. Eng. Data 57 (11), 3032–3091. https://doi.org/10.1021/je300655b.

Lemmon, E.W., Bell, I.H., Huber, M.L., McLinden, M.O., 2018. NIST Standard Reference Database 23: Reference Fluid Thermodynamic and Transport Properties-REFPROP, Version 10.0.

Li, H., Wu, Y., Zeng, X., Wang, X., Zhao, D., 2017. Property evaluations of hydrocarbon fuels under supercritical conditions based on cubic equation of state. Mod. Phys. Lett. B 31 (16), 1750164. https://doi.org/10.1142/S0217984917501640.

Lopez-Echeverry, J.S., Reif-Acherman, S., Araujo-Lopez, E., 2017. Peng-Robinson equation of state: 40 years through cubics. Fluid Phase Equil. 447, 39–71. https://doi.org/10.1016/j.fluid.2017.05.007.

Mangold, F., Pilz, St, Bjelic, S., Vogel, F., 2019. Equation of state and thermodynamic properties for mixtures of $H_2O$, $O_2$, $N_2$, and $CO_2$ from ambient up to 1000 K and 280 MPa. J. Supercrit. Fluids 153, 104476. https://doi.org/10.1016/j.supflu.2019.02.016.

Marsh, K., Perkins, R.A., Ramires, M.L., 2002. Measurement and correlation of the thermal conductivity of propane from 86 L to 600 K at pressures to 70 MPa. J. Chem. Eng. Data 47 (4), 932–940. https://doi.org/10.1021/je010001m.

Matheis, J., Hickel, S., 2018. Multi-component vapor-liquid equilibrium model for LES of high-pressure fuel injection and application to ECN Spray A. Int. J. Multiphas. Flow 99, 294–311. https://doi.org/10.1016/j.ijmultiphaseflow.2017.11.001.

Mazurek, D.M., Anderson, P.S., 1994. Application of Ultra-high Pressure Dense Phase Pipelines to Large Diameter Transmission Systems. NOVA Gas Int. Seminars, Kuala Lumpur, Malaysia.

Mokhatab, S., Poe, W.A., Mak, J.Y., 2019. Handbook of Natural Gas Transmission and Processing-Principles and Practices, fourth ed. Gulf Professional Publishing, Elsevier, Inc. (Chapter 1).

Moosavi, M., Abareshi, M., 2012. High temperature-high pressure density prediction of hydrocarbon systems using an extended LJ potential-based equation of state. J. Supercrit. Fluids 68, 71–80. https://doi.org/10.1016/j.supflu.2012.04.011.

Moshfeghian, M., 2009. Variation of Properties in the Dense Phase Region; Part 1– Pure Compounds. PetroSkills. http://www.jmcampbell.com/tip-of-the-month/2009/12/variation-of-properties-in-the-dense-phase-region-part-1-pure-compounds/. (Accessed 9 January 2023).

Moshfeghian, M., 2010. Variation of Properties in the Dense Phase Region; Part 2 – Natural Gas. PetroSkills. http://www.jmcampbell.com/tip-of-the-month/2010/01/variation-of-properties-in-the-dense-phase-region-part-2-%E2%80%93-natural-gas/. (Accessed 9 January 2023).

Moshfeghian, M., Rajani, J., Snow-McGregor, K., 2022. Transport of Natural Gas in Dense Phase – Nord Stream I. PetroSkills. https://www.petroskills.com/en/blog

/entry/april2022-totm-Transportation-of-Natural-Gas-in-Dense-Phase%E2%80%93Nord-Stream-1. (Accessed 9 January 2023).
Nasrifar, K., 2010. Comparative study of eleven equations of state in predicting the thermodynamic properties of hydrogen. Int. J. Hydrogen Energy 35 (8), 3802–3811. https://doi.org/10.1016/j.ijhydene.2010.01.032.
Nord Stream, A.G.. The pipeline - Nord stream AG. http://www.nord-stream.com/the-project/pipeline/. Accessed 7 May 2023.
Passut, C.A., Danner, R.P., 1972. Correlation of ideal gas enthalpy, heat capacity and entropy. Ind. Eng. Chem. Process Des. Dev. 11 (4), 543–546. https://doi.org/10.1021/i260044a016.
Peng, D.-Y., Robinson, D.B., 1976. A new two-constant equation of state. Ind. Eng. Chem. Fundam. 15 (1), 59–64. https://doi.org/10.1021/i160057a011.
Perez, A.G., Coquelet, C., Paricaud, P., Chapoy, A., 2017, Comparative study of vapour-liquid equilibrium and density modelling of mixtures related to carbon capture and storage with the SRK, PR, PC-SAFT and SAFT-VR Mie equations of state for industrial uses. Fluid Phase Equil. 440, 19-35. https://doi.org/10.1016/j.fluid.2017.02.018.
Pioro, I., 2014. Applications of Supercritical Power Engineering: Specifics of Thermophysical Properties and Forced-Convection Heat Transfer. Supercritical Fluid Technology-For Energy and Environmental Application. Elsevier, ISBN 978-0-444-62696-7, pp. 201–233. https://doi.org/10.1016/C2012-0-00267-0. Ch. 11.
Poling, B.E., Prausnitz, J.M., O'Connell, J.P., 2000. The Properties of Gases and Liquids, fifth ed. McGraw-Hill, New York.
Prasad, V., Kakroo, K., Banerjee, D., 2022a. Existence of supercritical "liquid-like" state in subcritical region, optimal heat transfer enhancement, and argon as a nonreacting, noncorroding SC heat transfer fluid. Heat Tran. Res. 53 (9), 1–27. https://doi.org/10.1615/HeatTransRes.2022043095.
Prasad, V., Zhang, Z., Wang, G.X., Banerjee, D., Sadat, H., Bostanci, H., Almara, L.M., 2022b. Process and System for Heat Exchange Process. Patent Application No. 18/320,727, May 19, 2023, based on "Method and Systems using a Mixture of Supercritical Fluid Prepared Selectively for Heat Dissipation at Very-low to Very-high Temperatures and Pipeline Transport,". Provisional Patent No. 63/344,429 (05/20/2022).
Prasad, V., Wang, G.X., Zhang, Z., Banerjee John, H., Bostanci, H., Sadat, H., Almara, Prasad, LV, Wang, G.-X., John, K., Bostanci, H., Sadat, H., Almara, L., 2022c. Method and Conditions for Intra- and Inter-Continental Transport of Supercritical Natural Gas (SNG) via Pipelines through Land, Underground, Water Bodies, and/or Ocean. Provisional Patent, Application No. 63/375,085 (09/09/2022), Patent Application being submitted.
Prasad, V., Almara, L.M., Wang, G.X., 2023. Ultra-long-distance transport of supercritical natural gas (SNG) at high-mass flow rates via pipelines through land, underground, water bodies, and ocean. J. Natural Gas and Eng. 205053.
Ricci, D., Natale, P., Battista, F., 2016. Experimental and numerical investigation on the behavior of methane in supercritical conditions. Appl. Therm. Eng. 107, 1334–1353. https://doi.org/10.1016/j.applthermaleng.2016.07.052.
Setzmann, U., Wagner, W., 1991. A new equation of state and tables of thermodynamic properties for methane covering the range from the melting line to 625 K at pressures up to 1000 MPa. J. Phys. Chem. Ref. Data 20, 1061–1155. https://doi.org/10.1063/1.555898.
Soave, G., 1972. Equilibrium constants from a modified Redlich-Kwong equation of state. Chem. Eng. Sci. 27 (6), 1197–1203. https://doi.org/10.1016/0009-2509(72)80096-4.
Vargas-Vera, B.H., Rada-Santaigo, A.M., Cabarcas-Simanacas, M.E., 2020. Gas transport at dense phase conditions for the development of deepwater fields in the Colombian Caribbean Sea. Ciencia, Tecnologia y Futuro 10, 17–32. https://doi.org/10.29047/01225383.131.
Votta, R., Battista, F., Salvatore, V., Pizzarelli, M., Leccese, G., Nasuti, F., Meyer, S., 2016. Experimental investigation of transcritical methane flow in rocket engine cooling channel. Appl. Therm. Eng. 101, 61–70. https://doi.org/10.1016/j.applthermaleng.2015.12.019.
Younglove, B.A., Ely, J.F., 1987. Thermophysical properties of fluids. II. Methane, ethane, propane, isobutane, and normal butane. J. Phys. Chem. Ref. Data 16, 577. https://doi.org/10.1063/1.555785.
Zhang, P., Zhou, L., Zeng, W., Xiong, G., Huang, H., Cai, L., Ye, H., Qu, S., 2020. Hydrocarbon dew point measurement and model evaluation of synthetic and real natural gases. ACS Omega 5 (15). https://doi.org/10.1021/acsomega.9b03469, 8463−8473.
Zivdar, M., Abofarakh, M., 2021. Natural gas transmission in dense phase mode. J. Gas Technology 7 (2), 45–52. DOR: 20.1001.1.25885596.2021.7.2.4.6.